Potential of polarizable force fields for predicting the separation performance of small hydrocarbons in M-MOF-74

Becker, Tim M.; Luna-Triguero, Azahara; Vicent-Luna, Jose Manuel; Lin, Li Chiang; Dubbeldam, David; Calero, Sofia; Vlugt, Thijs J.H.

DOI
10.1039/c8cp05750h

Publication date
2018

Document Version
Accepted author manuscript

Published in
Physical chemistry chemical physics (PCCP)

Journal Name

ARTICLE TYPE

Cite this: DOI: 10.1039/xxxxxxxxxx

Potential of Polarizable Force Fields for Predicting the Separation Performance of Small Hydrocarbons in M-MOF-74†

Tim M. Becker,[a] Azahara Luna-Triguero,[b] Jose Manuel Vicent-Luna,[b] Li-Chiang Lin,[c] David Dubbeldam,[d] Sofia Calero,[b] and Thijs J. H. Vlugt*[a]

Received Date
Accepted Date

DOI: 10.1039/xxxxxxxxxx

www.rsc.org/journalname

The separation of light olefins from paraffins via cryogenic distillation is a very energy intensive process. Solid adsorbents and especially Metal-Organic Frameworks with open metal sites have the potential to significantly lower the required energy. Specifically, M-MOF-74 has drawn considerable attention for application in olefin/paraffin separation. To investigate how the separation proceeds on a molecular level and to design better materials, molecular simulation can be a useful tool. Unfortunately, it is still a challenge to model the adsorption behavior of many adsorbates in Metal-Organic Frameworks with open metal sites. Previously, the inclusion of explicit polarization has been suggested to improve the quality of classical force fields for such systems. Here, the potential of polarizable force fields for the description of olefins and paraffins in Metal-Organic Frameworks with open metal sites is investigated. In particular, heats of adsorption, binding geometries, and adsorption isotherms are calculated for C_2H_4, C_2H_6, C_3H_6, and C_3H_8 in M-MOF-74 (with M = Co, Mn, Fe, and Ni). In this study, no force field parameters are adjusted to improve the model. The results show that including explicit polarization significantly improves the description of the adsorption in comparison to non-polarizable generic force fields which do not consider explicit polarization. The study also reveals that simulation predictions are sensitive to the assigned repulsive potential and framework charges. A fully re-parametrized polarizable force field may have the capability to improve the predictions even further.

1 Introduction

The separation of light olefins and paraffins is one of the major large scale processes in the petrochemical industry[2,3]. Light paraffins are mainly used for heating while olefins are important raw chemicals. For instance, the production of polymers requires a high purity of olefins[2]. Conventionally, light hydrocarbons are separated after cracking of long chain hydrocarbons in cryogenic distillation. The product of the cracking at elevated temperatures has to be cooled down to the low boiling points of the light hydrocarbons[4] (e.g., ethane: 184.5 K, propane: 231.1 K[5]). This makes cryogenic distillation a very cost intensive process both energy and investment wise and alternatives have been investigated for decades[6]. A more cost and energy efficient separation of light hydrocarbons is also crucial for the purification of natural gas[7], which has to be realized economically on a smaller scale[8].

Solid adsorbents can be operated at intermediate temperatures. Thereby, they have the potential to drastically lower the energy required to separate light olefins from paraffins by avoiding the cooling necessary in cryogenic distillation[2,5,9–11]. Traditionally, the separation of light olefins via physical adsorption has not been considered promising due to low uptake capacities[6]. This limitation might be surmountable by Metal-Organic Frameworks (MOFs). This emerging type of porous material can be customized to satisfy chosen applications[12]. The family of M-MOF-74 (where M can be substituted by a variety of first row transition metals or Mg) has been extensively investigated[13–19] due to its large surface area which includes a high density of open metal

[a] Engineering Thermodynamics, Process & Energy Department, Faculty of Mechanical, Maritime and Materials Engineering, Delft University of Technology, Leeghwaterstraat 39, 2628CB Delft, The Netherlands. E-mail: T.J.H.Vlugt@tudelft.nl
[b] Department of Physical, Chemical and Natural Systems, Universidad Pablo de Olavide, Ctra. Utrera km 1. ES-41013, Seville, Spain.
[c] William G. Lowrie Department of Chemical and Biomolecular Engineering, The Ohio State University, 151 W. Woodruff Ave., Columbus, OH 43210, United States.
[d] Van't Hoff Institute for Molecular Sciences, University of Amsterdam, Science Park 904, 1098XH Amsterdam, The Netherlands.

† Electronic Supplementary Information (ESI) available: Tables containing force field parameters of all investigated force fields; schematic representation of binding geometry for C3 hydrocarbons; computed binding geometries for all investigated systems; adsorption isotherms calculated with the force field of Liu *et al.* [1] with addition explicit polarization; heats of adsorption and adsorption isotherms calculated for Co-MOF-74 with QEq charges; energy surfaces of Co-MOF-74 for the maximum energy plane in z-direction. See DOI: 10.1039/b000000x/

sites[20]. Zn-MOF-74 was first reported in 2005[21], and isostructural systems with other metal centers have been subsequently synthesized (Co, Cu, Fe, Mg, Mn, and Ni)[22–27]. Open metal sites interact more strongly with unsaturated hydrocarbons than with saturated hydrocarbons[28–30]. In an adsorption process, M-MOF-74 has the potential to achieve the high selectivities and large uptakes required by industry[2,8]. Several experimental studies have been conducted and confirm that M-MOF-74 is indeed able to fractionate multicomponent hydrocarbon mixtures[2,5,8,31–33], as well as other gases[13,15,31,34–36].

A recent first-principle simulation study suggests that π bonding, polarization, and strong dispersion interactions between the olefins and the open metal sites are accountable for the high uptake of olefins[32]. In addition, dipole and quadrupole interactions have been demonstrated to play an important role[37,38]. Molecular simulation offers the possibility to further investigate the underlying mechanisms of the separation[39]. A fundamental understanding can help to rationally design MOFs with customized properties for enhanced performance[40,41]. However, it is challenging to capture the adsorption behavior of MOFs with open metal sites and further research is required[11,41–43]. The main question to address is how to incorporate the enhanced interactions of olefins with open metal sites. From a research perspective, the family of M-MOF-74 is a perfect candidate to examine this question, because the influence of varying cations acting as open metal sites can be investigated using a series of isoreticular structures[7,31,34,38]. Several molecular simulation studies considering light hydrocarbons in M-MOF-74 have already been conducted[11,37,44]. However, generic force fields are known to be inadequate[42,43,45,46] and until now customized force field seem to be the only solution for these systems.

This study aims to investigate the potential of polarizable force field to describe the different adsorption behavior of ethane, ethylene, propane, and propylene in MOFs with open metal sites. Force fields developed by others[47,48] which include point charges are used for ethylene and propylene to reproduce the static quadrupole and dipole moments, respectively. The non-iterative induced dipole procedure of Lachet *et al.*[49] is applied to consider polarization explicitly. Point polarizabilities are taken from literature and are added to the atom sites of all investigated molecules. To obtain an unbiased understanding of the potential of polarizable force fields for the description of light olefins and paraffins, no adjustments of the force field parameters are made to improve the results. With the polarizable model, heats of adsorption, binding geometries, and adsorption isotherms are calculated and compared to already existing force fields and experimental data. Subsequently, the influence of individual energy contributions and the effect of different sets of framework charges are discussed. Finally, the performance of the new model including polarization is evaluated, difficulties are reported and possibilities for further improvement are highlighted.

2 Background

The force field development of olefins and paraffins in MOFs with open metal sites is particularly challenging[11,41,43]. The model has to describe differences in adsorption for molecules with comparable size and chemical composition[5,6,50]. Examples of such force fields are the TraPPE force field[51] and the force field of Liu *et al.*[1], which are unable to capture the physical difference between olefins and paraffins in MOFs with open metal sites. A common approach to overcome the limitations of such force fields is to adjust the Lennard-Jones mixing rules between framework and adsorbate. Luna-Triguero *et al.*[44] adjusted the mixing rules and thereby developed a force field which describes the adsorption of light hydrocarbons in M-MOF-74 well. Unfortunately, force fields that are created in this fashion are usually not transferable to other systems[44]. Generic force fields that do not include point charges nor explicit polarization seem to fail in an environment in which localized electrostatic effects occur as in the case of M-MOF-74[42,52,53].

A more physically motivated approach to model the difference in adsorption behavior between olefins and paraffins could be to include point charges and explicit polarization[41]. To the best of our knowledge, none of the currently available models considers explicit polarization successfully for these molecules in MOFs[1,41,47,48,51,54]. Furthermore, many force fields do not take into account the difference in charge distribution between olefins and paraffins explicitly. The polarizability of olefins and paraffins is similar while the permanent multipole moments are much stronger for olefins[5]. Still, it has been suggested that a combined effect between polarization and electrostatics might be crucial to model the adsorption behavior in MOFs with open metal sites and that considering exclusively electrostatics is not sufficient[42,53]. In molecular simulation most commonly, point charges are assigned to molecules to reproduce multipole moments[55]. These multipole moments can be predicted from quantum mechanics (QM), determined via experiments, or fitted to reproduce experimental data[55,56]. For olefins and paraffins, the common approach is to add point charges to olefins, but not for paraffins[47,48,57]. Such models are chosen here. Besides the adsorbates, charges need to be considered for the frameworks. Various approaches exist to consider polarization, i.e., the induced dipole method, the shell method, and the fluctuating charge method[58,59]. These approaches have the potential to improve the modeling and force field transferability, especially for systems with localized electrostatic interactions[42,60]. Due to high computational costs in Monte Carlo simulations, studies investigating polarizable force fields are rather limited[61]. McDaniel *et al.*[40] used the shell model to create a polarizable force field for CO_2 in several ZIFs,[40,62] and for CO_2 and CH_4 in MOFs[63]. In addition to explicit polarization, these authors completely re-parameterized framework-adsorbate interactions to reproduce results from QM. The resulting force fields described the experimental adsorption accurately. Unfortunately, the simulations which considered explicit polarization took at least 2 to 10 times longer than standard Monte Carlo simulations. Moreover, the group of Space *et al.* applied the induced dipole method to describe adsorption in MOFs with open metal sites[41,42,52,53,64–67]. The early work of these authors focused on the adsorption of H_2 in MOFs with open metal sites[42,52,53,64,65]. Later, the group studied polarizable force fields for CO_2[41,66,67] and with less accuracy C2 hydrocarbons[41]. The studies show that considering explicit polarization significantly improved the

description of adsorption in MOFs with open metal sites. The drawback is that explicit polarization accounted for as much as 95% of the total computational time.

In this study, the induced dipole method is also adopted[58,59] to account for polarization. As in our previous work[61,68,69], additional approximations and assumptions are made. These simplifications were first introduced by Lachet *et al.*[49] to model xylenes in NaY zeolite and drastically speed up the calculations. To reduce the computational costs of the method, exclusively induced dipole moments are considered, a linear response between isolated point dipoles and the electric field is assumed, and back-polarization is neglected. Furthermore, polarization is only considered between the MOF framework and adsorbates. Polarization between adsorbate molecules is not explicitly considered, because the vapor-liquid equilibrium of these molecules is already described well by the chosen force fields[70]. Due to the negligence of back-polarization and the consideration of polarization exclusively between framework and adsorbates, induced dipoles μ_i can be calculated according to[49]:

$$\mu_i = \alpha_i \cdot \mathbf{E}_i^0, \tag{1}$$

where α_i and $\mathbf{E}_i^0$ are the static dipole polarizability and the electric field created by the framework at the interaction site i. Accordingly, the energy contribution of polarization can be calculated from the static electric field created by the framework[61] when static dipole polarizabilities are assigned to interaction sites. Hence, the induction energy U_{ind} can be determined from[49]:

$$U_{\text{ind}} = -\frac{1}{2}\sum_{i=1}^{n} \alpha_i \cdot \left|\mathbf{E}_i^0\right|^2, \tag{2}$$

where n is the total amount of interaction sites that have been changed in the respective Monte Carlo step. The required simulation time is comparable to that without considering explicit polarization. The remaining contributions to the total energy are the energies which result from the Lennard-Jones potential and from electrostatic interactions between point charges ($U_{\text{total}} = U_{\text{LJ}} + U_{\text{el}} + U_{\text{ind}}$). Previously, we successfully used the approach to describe the adsorption of CO_2 in M-MOF-74[61,68] with a variety of different metal atoms. Details of the simulation procedure are explained in the work of Lachet *et al.*[49] and our previous studies[61,68]. It is important to note that in this study no fitting parameters are used and that the computational results are pure predictions.

3 Simulation details

The RASPA software package[71,72] is used to conduct grand-canonical Monte Carlo simulations and to compute the absolute uptake of ethane, ethylene, propane, and propylene in several structures of M-MOF-74 (M = Co, Mn, Fe, and Ni). The pure component uptakes are computed for varying fugacities at 318 K and for pressures up to 8 bar. Heats of adsorption at infinite dilution are determined from energy differences in the *NVT* ensemble[73]. In addition, *NVT* Monte Carlo simulations are conducted to determine the binding geometry of all adsorbate molecules in M-MOF-74. A simulated annealing procedure is used to find the position corresponding to the global energy minimum. MOF crystal structures for Co-MOF-74, Fe-MOF-74, Mn-MOF-74, and Ni-MOF-74 are taken from Dietzel *et al.*[22], Bloch *et al.*[35], Zhou *et al.*[24], and Dietzel *et al.*[23], respectively, while atomic charges are assigned according to DFT calculations and are taken from the work of Lee *et al.*[38] and Mercado *et al.*[7] . The positions of the framework atoms are considered to be fixed. Lennard-Jones parameters for paraffins are taken from the TraPPE force field[51] and for ethylene and propylene from Lahoz-Martín *et al.*[48] and Gutiérrez-Sevillano *et al.*[47], respectively. Interactions between adsorbates are not modified and computed based on the original force fields. Force field parameters of the DREIDING force field are assigned to carbon, oxygen, and hydrogen atoms of M-MOF-74[74]. Lennard-Jones parameters of Co, Mn, Fe, and Ni are taken from the UFF force field[75]. Cross-interactions are determined via the Lorentz-Berthelot mixing rule[76,77]. The Lennard-Jones potential is truncated at a cutoff distance of 12 Å without tail corrections. Periodic boundary conditions are applied in all directions to mimic the behavior of a continuous system. The simulated systems are composed of 2x2x4 unit cells to ensure a minimum distance of more than twice the cutoff radius between periodic images. The Ewald summation technique with a relative precision of 10^{-6} is used to calculate electrostatic interactions between static point charges[39]. Explicit polarization is considered via the induced dipole method[58] with additional assumptions introduced by Lachet *et al.*[49]. As noted above, polarization is exclusively considered between the framework and adsorbate molecules. Back-polarization is neglected to achieve reasonable simulation times. The required atomic polarizabilties α_i are taken from Stout and Dykstra[78]. All force field parameters are summarized in the Electronic Supplementary Information (ESI). For comparison with experimental results and reported simulations results, the Peng-Robinson equation of state is used to convert fugacities to pressures[79].

4 Results and discussion

To verify how inclusion of polarization influences the description of small hydrocarbons in M-MOF-74, heats of adsorption at infinite dilution, binding geometries, and adsorption isotherms are investigated. The heat of adsorption is a measure of the interaction strength between adsorbates and the framework[67,73]. Here, heats of adsorption at infinite dilution are compared with values derived from experimental adsorption isotherm at different temperatures using the Clausius-Clapeyron equation[5,80]. Although, heats of adsorption derived from the Clausius-Clapeyron equation are sensitive towards small changes in the adsorption isotherms[67], comparison with the Clausius-Clapeyron equation to assess the quality of molecular simulation in the absence of experimental measurements is useful. To systematically investigate the influence of point charges and explicit polarization, heats of adsorption are calculated with force fields that incorporate these features fully, partially, or not at all. Force fields that neither consider point charges nor polarization are the force field of Liu *et al.*[1] and the TraPPE force field[51]. In this study, the force field that exclusively considers point charges for olefins is named *no polarization* and the one that solely considers explicit polariza-

tion is refered to as *no charges*. The force field that considers both charges and polarization is called *pol. force field*. The calculated heats of adsorption for these force field are presented in Figure 1 for ethane, ethylene, propane, and propylene in (a) Co-MOF-74, (b) Fe-MOF-74, (c) Mn-MOF-74, and (d) Ni-MOF-74.

Since no point charges are assigned to paraffins, the force fields *no charges* and the force field of Liu *et al.* [1], and *no polarization* and the polarizable force field are equivalent for ethane and propane. The heats of adsorption determined with the Clausius-Clapeyron equation from experiments show strong affinity between the oleffins and all investigated M-MOF-74 frameworks [2,5,8]. The binding energies predicted by Lee *et al.* [38] display larger differences between the individual frameworks. According to the results of these authors, especially the behavior of propane in the different frameworks varies. In this study, the computed heats of adsorption show that neither the force field considering solely charges (*no polarization*) nor the one considering solely polarization (*no charges*) can reproduce the experimental trend. The force field of Liu *et al.* [1] and the TraPPE force field [51] show the opposite behavior to experiments, i.e., a higher affinity for paraffins. Adding solely polarization simply increases the interactions for both paraffins and olefins. Moreover, inclusion of charges without polarization does not increase the binding affinity of the olefins sufficiently to reproduce the expected trend. In sharp contrast to including either point charges or explicit polarization, when considering both, the calculated heats of adsorption follow the experimental trend. A large synergy effect between electrostatic interactions and polarization can be observed. This synergy effect significantly increases the calculated heats of adsorption for olefins. Similar effects have been previously observed by Forrest *et al.* [42] and Pham *et al.* [53]. For the polarizable force field, differences can be observed between Co-MOF-74 and Ni-MOF-74, and Fe-MOF-74 and Mn-MOF-74. In the case of Fe-MOF-74 and Mn-MOF-74, the affinity of the oleffins is more pronounced. For Co-MOF-74 and Ni-MOF-74, the polarizable force field predicts lower heats of adsorption for ethylene and propylene in comparison to the predictions from the Clausius-Clapeyron equation. Nevertheless, it is evident that considering polarization together with point charges for olefins significantly improves the capability of the force field to describe heats of adsorption in M-MOF-74. The polarizable force field has the capability to model the larger adsorption strength for olefins. No perfect quantitative agreement with experiments can be expected, since the improvement in the description was achieved by simply adding explicit polarization to the model of the adsorbates without further adjusting any force field parameters. Analogously to the observation of Franz *et al.* [41], in this study the predicted energetics for low uptakes seem to be better modeled when considering polarization.

In previous studies of others [2,11,38], the stronger binding of olefins over paraffins has been ascribed to interactions between the double bond of olefins and open metal sites of the MOF. Some authors suggest that the double bond of olefins is located parallel to the open metal site, while paraffins bind with one side pointing towards the open metal sites [2,5]. These adsorption geometries can be examined in molecular simulation. A simulated annealing procedure is conducted to determine the lowest energy binding geometries. The results are compared to geometries predicted in DFT calculations performed by Lee *et al.* [38]. The binding geometry is reported according to Figure 2.

Three parameters l_1, α, and β are used to quantify the binding geometry. l_1 is the distance between the site of the adsorbate closest to the open metal site and the open metal site. α is the angle between the bond of the adsorbate and l_1, while β is the angle between l_1 and the bond between the open metal site and the out of plane oxygen atom. For C3 hydrocarbons the labeling is analogous, to the exclusion of an additional carbon site that is connected to the carbon site further away from the metal. A schematic representation for C3 hydrocarbons is provided in the ESI. For a binding geometry in which the double bond between the carbons is located parallel to the open metal site, α and β should be approximately 90° and 170°, respectively (expected for olefins [2,5]). If the adsorbate is directed with one side towards the open metal site α should be larger than 90° (expected for paraffins [2,5]). The determined binding geometries of the lowest energy configurations in Co-MOF-74 are summarized in Figure 3 for (a) ethylene, (b) propylene, (c) ethane, and (d) propane, and compared to lowest energy positions determined in DFT calculations of Lee *et al.* [38]. The geometries determined with the polarizable force field agree well with the previously suggested binding geometries [2,5]. Distinct differences can be observed between olefins and paraffins. β is close to 170° for all adsorbates, while α is approximately 90° for the olefins and 120° for the paraffins. This shows that the olefins described by the polarizable force field indeed bind with the double bond parallel to the open metal sites. The force field not considering polarization but including point charges (*no polarization*) predicts very similar angles for the olefins. Hence, point charges for olefins seem to be crucial to model the orientation of the adsorbates. For propane, the polarizable force field predicts an α of approximately 120° in agreement with our expectations (one side of the molecule is pointing towards the open metal site). The force field of Liu *et al.* [1] and the TraPPE force field predict configurations for propane in which one bond is arranged parallel to the open metal site. Apparently, the inclusion of polarization influences the binding geometry of propane positively. Overall, the force fields not considering polarization nor point charges (Liu *et al.* [1], TraPPE [51]) predict binding geometries that vary from the predicted trends for ethylene, propane, and propylene. DFT results of Lee *et al.* [38] for olefins are comparable to the predictions with the polarizable force field. For propane, Lee *et al.* [38] reports that these calculations might have been stuck in a local energy minimum which could explain some deviations. The DFT results suggest that exclusively the distance l_1 is larger for ethane than for ethylene and that the carbon bond of both molecules is located parallel towards the open metal site. Due to generally high sensitivity of binding geometries towards the applied force field some uncertainties are expected. Issues can easily arise if interactions are strong and adsorbates are located close to the surface of the framework, as for MOFs with open metal sites. The other investigated M-MOF-74 frameworks show a behavior similar to Co-MOF-74. Deviations from the expected configurations can only be observed for propylene in Mn-MOF-74 and propane in Ni-MOF-74. The corresponding figures

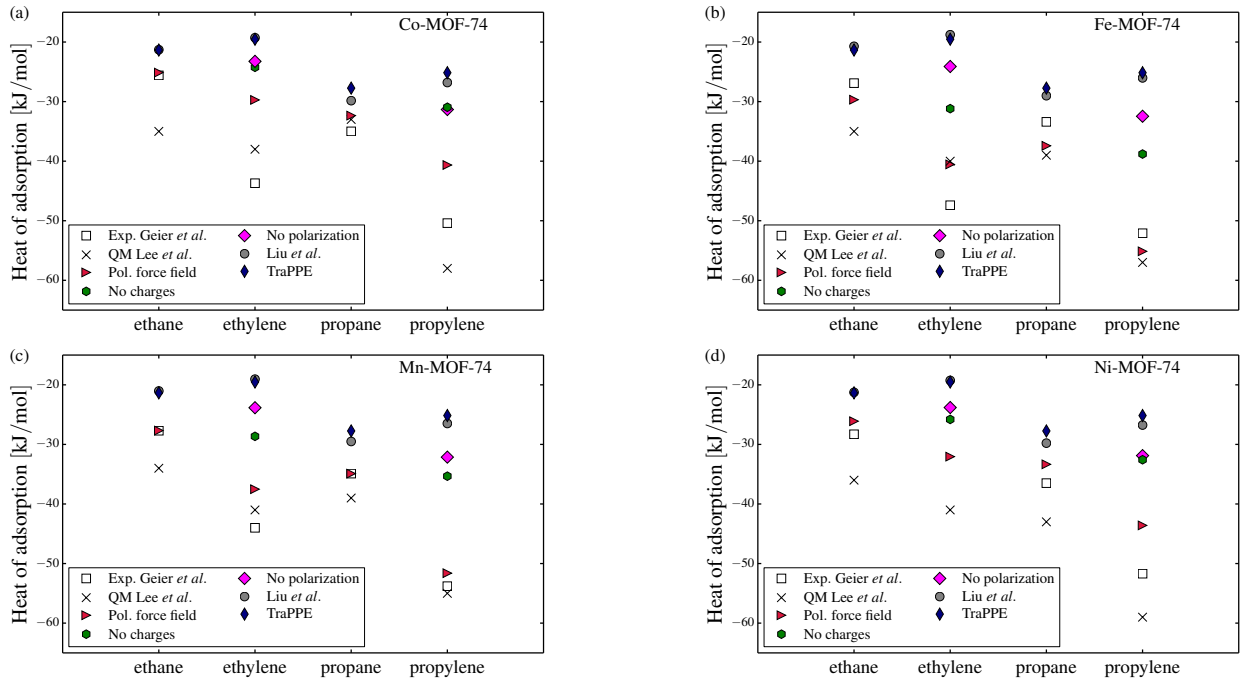

Fig. 1 Heats of adsorption at infinite dilution calculated using various force fields at 318 K for (a) Co-MOF-74, (b) Fe-MOF-74, (c) Mn-MOF-74, and (d) Ni-MOF-74. The computational results are compared to DFT binding energies from Lee *et al.*[38] and heats of adsorption predicted via the Clausius-Clapeyron equation from experiments by Geier *et al.*[5].

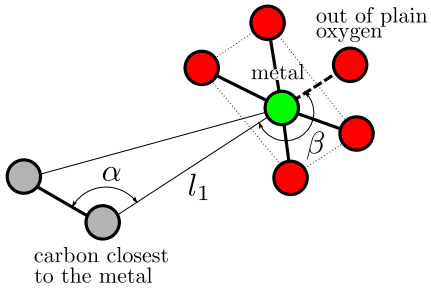

Fig. 2 Schematic representation of the binding geometry for C2 hydrocarbons within M-MOF-74. Carbon atoms, the metal atom, and oxygen atoms are colored in grey, green, and red, respectively.

are included in the ESI. In summary, it is apparent that the inclusion of point charges and polarization leads to an improvement in the modeling of the binding geometry. Together with the improvements for the heats of adsorption, this is a very reassuring finding, since the description of the adsorption behavior at low uptakes is significantly improved by the polarizable model without introducing any adjustable parameters. These findings verify the need for polarizable force fields.

After considering the low uptake adsorption, it is of interest to investigate adsorption isotherms which are also influenced by adsorbate-adsorbate interactions and the packing within the pores[42]. Computed adsorption isotherms are compared to experimental measurements of Geier *et al.*[5]. These authors provide a complete set of experimental adsorption isotherms for the MOF structures and adsorbates considered. For some MOFs additional experiments are available[2,8]. As previously shown[44], these experiments agree well with the study of Geier *et al.*[5]. To increase the visibility, exclusively the measurements of Geier *et al.*[5] are presented as comparison. Due to the limited amount of experimental studies, a thorough investigation of the reproducibility of the experimental adsorption isotherms as suggested by Park *et al.*[81] is not possible. Hence, the experimental values should rather be seen as guidelines and not as final target. In Figure 4, the computed adsorption isotherms of ethane are compared to experimental results of Geier *et al.*[5] for (a) Co-MOF-74, (b) Fe-MOF-74, (c) Mn-MOF-74, and (d) Ni-MOF-74 at 318 K.

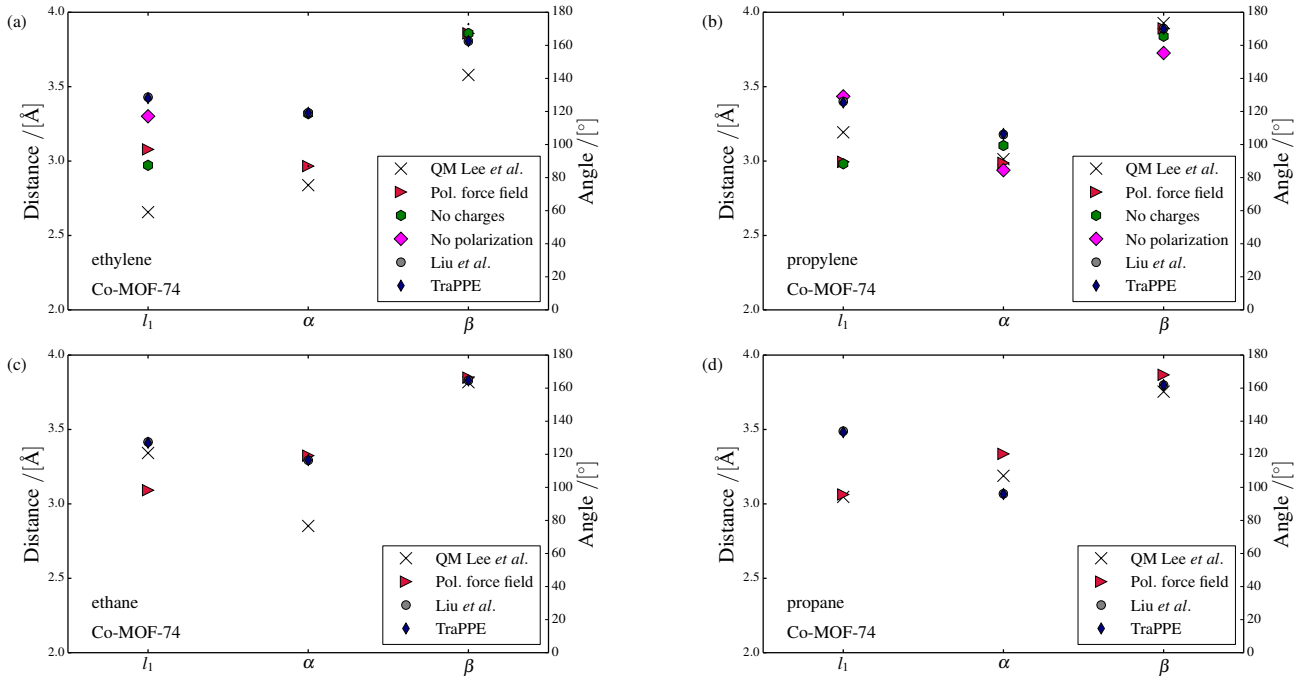

Fig. 3 Summary of parameters to describe the binding geometry of (a) ethylene, (b) propylene, (c) ethane, and (d) propane in Co-MOF-74. Comparison between several classical force fields and the DFT results of Lee *et al.* [38]. Parameters are defined according to Figure 2.

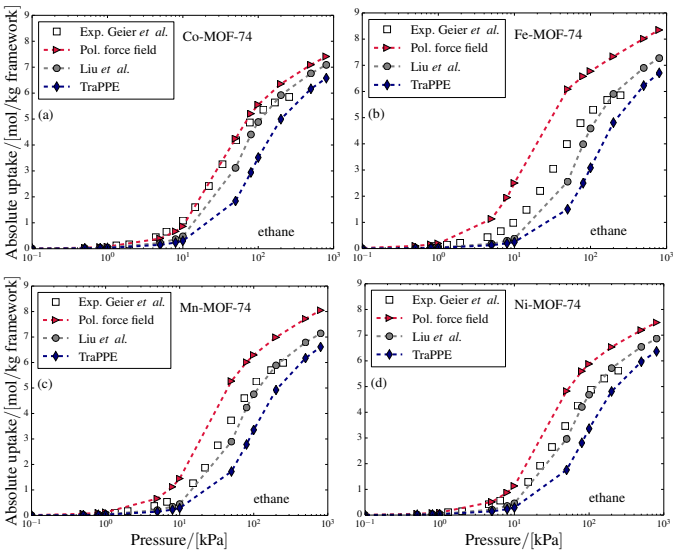

Fig. 4 Comparison of adsorption isotherms of ethane for (a) Co-MOF-74, (b) Fe-MOF-74, (c) Mn-MOF-74, and (d) Ni-MOF-74 at 318 K between the experimental values of Geier *et al.* [5] and simulation results using the force fields of Liu *et al.* [1], the TraPPE force field [51], and the developed polarizable force field.

In agreement with the heats of adsorption and the binding geometries, the low pressure region is improved when adding explicit polarization. The uptake at higher values of pressure is overestimated. This could be due to oversized dispersion interactions of standard force fields and an adjustment of Lennard-Jones parameters might be required for accuracy [41]. However, an overprediction of the uptake at high pressure is frequently observed in molecular simulation and therefore not surprising [82]. Besides the force field, possible reasons can be imperfect crystal structures for the synthesized material or collapsed and blocked cavities in experiments [14,83]. Adsorption at high pressure is dominated by molecule packing inside the pores and not by specific framework-adsorbate interactions [42,84]. To describe the packing behavior of molecules, adsorbate-adsorbate interactions are more important than the adsorbate-framework interactions which are influenced by the developed polarizable force field. To achieve a better agreement between experiments and molecular simulation at high pressure many studies apply a constant factor to scale the computational adsorption isotherm [7,18,81]. In this study, scaling is avoided to achieve an unbiased evaluation of the potential of polarizable force fields for small hydrocarbons. For ethane, the presented polarizable force field is created by adding explicit polarization to the TraPPE force field [51]. The TraPPE force field without considering explicit polarization underestimates the uptake in the investigated frameworks. Besides the polarizable force field, the force field of Liu *et al.* [1] performs well. This force field was fitted to reproduce the adsorption of hydrocarbons in zeolites. The conditions in zeolites and MOFs may be similar for paraffins, because these molecules do not interact strongly with open metal sites. Hence, the adjustment for zeolites might result in good agreement for MOFs. If polarization is simply added to the force field of Liu *et al.* [1], the uptake is largely overestimated. The corresponding adsorption isotherms can be found in the ESI. Figure 5 compares the computed adsorption isotherms for ethylene in (a) Co-MOF-74, (b) Fe-MOF-74, (c) Mn-MOF-74, and (d) Ni-MOF-74 with the experimental values from Geier *et al.* [5] at 318 K.

For ethylene, the developed polarizable force field performs the best in all 4 M-MOF-74 frameworks. The force fields without con-

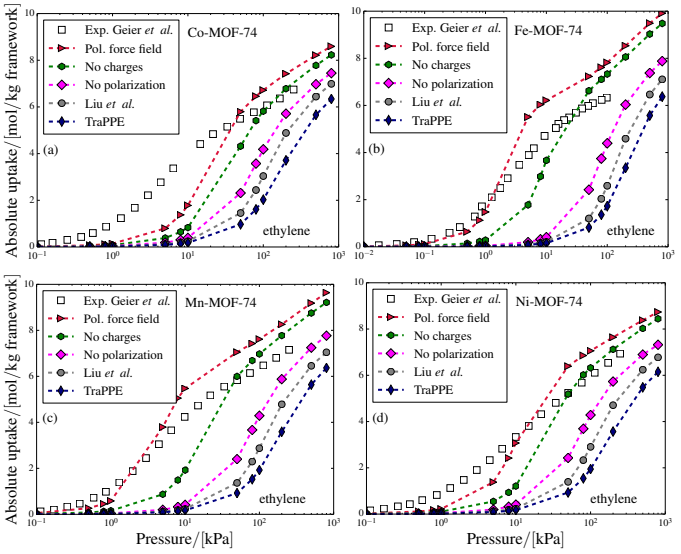

Fig. 5 Comparison of adsorption isotherms of ethylene for (a) Co-MOF-74, (b) Fe-MOF-74, (c) Mn-MOF-74, and (d) Ni-MOF-74 at 318 K between the experimental values of Geier *et al.*[5] and simulation results using the force field of Liu *et al.*[1], the TraPPE force field[51], a force field without point charges (*no charges*), a force field without polarization (*no polarization*), and the developed polarizable force field.

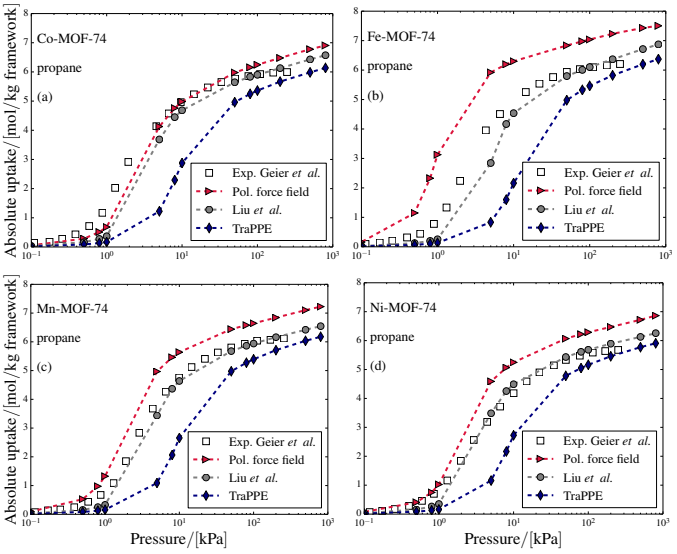

Fig. 6 Comparison of adsorption isotherms of propane for (a) Co-MOF-74, (b) Fe-MOF-74, (c) Mn-MOF-74, and (d) Ni-MOF-74 at 318 K between the experimental values of Geier *et al.*[5] and simulation results using the force fields of Liu *et al.*[1], the TraPPE force field[51], and the developed polarizable force field.

sidering polarization fail to predict even the qualitative adsorption behavior. Neither the TraPPE force field[51] nor the force field of Liu *et al.*[1] can capture the behavior of experimentally measured adsorption isotherms. In contrast to ethane, for ethylene the force field of Liu *et al.*[1] performs poorly. The difference could be caused by the strong interactions of olefins with the open metal sites. These interactions are not present in zeolites and therefore not captured in the force field of Liu *et al.*[1]. The agreement between the polarizable force field and the experimental results is the poorest for Co-MOF-74. The important low pressure region is underpredicted for Co-MOF-74. This underprediction agrees with the underestimation for the heat of adsorption at infinite dilution of ethylene in Co-MOF-74 (cf. Figure 1). A less pronounced disagreement between experiments and simulations at low pressure can be observed for Ni-MOF-74. Unfortunately, no experimentally derived value for the heat of adsorption is available for ethylene in Ni-MOF-74. For Fe-MOF-74 and Mn-MOF-74, the agreement at low pressure is good while the adsorption at high pressure is overpredicted. Figure 6 shows the computed adsorption isotherms for propane and experimental isotherms of Geier *et al.*[5] for (a) Co-MOF-74, (b) Fe-MOF-74, (c) Mn-MOF-74, and (d) Ni-MOF-74 at 318 K.

The observations for propane are very similar to the findings for ethane. The agreement between experiments and simulations is very good for Co-MOF-74, while simulation overestimates the uptake for Fe-MOF-74. For Mn and Ni based frameworks, adsorption at low pressure is well reproduced. With the TraPPE force field[51] the uptake in all frameworks is severely underestimated. In contrast, the force field of Liu *et al.*[1] predicts adsorption well. In Figure 7 the computed adsorption isotherms for propylene in (a) Co-MOF-74, (b) Fe-MOF-74, (c) Mn-MOF-74, and (d) Ni-MOF-74 are compared to experiments of Geier *et al.*[5] at 318 K.

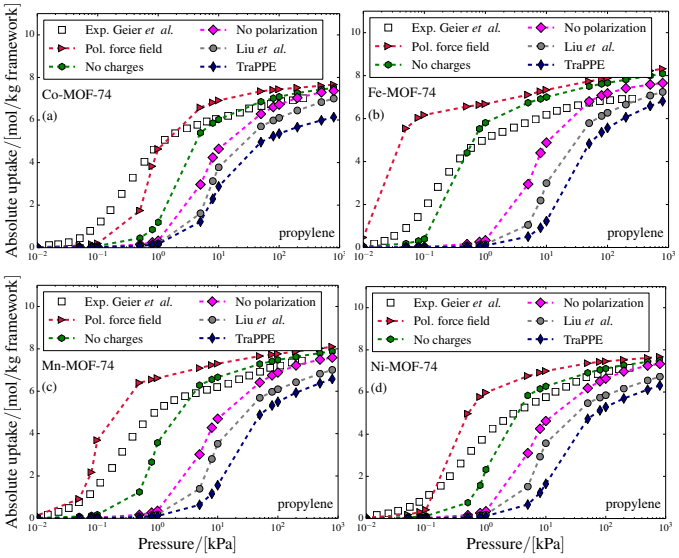

Fig. 7 Comparison of adsorption isotherms of propylene for (a) Co-MOF-74, (b) Fe-MOF-74, (c) Mn-MOF-74, and (d) Ni-MOF-74 at 318 K between the experimental values of Geier *et al.*[5] and simulation results using the force field of Liu *et al.*[1], the TraPPE force field[51], a force field without point charges (*no charges*), a force field without polarization (*no polarization*), and the developed polarizable force field.

The predicted adsorption isotherms for propylene calculated with force fields that do not consider polarization (Liu *et al.*[1], TraPPE[51], and *no polarization*) underestimate the experimental update significantly and exhibit different shapes in comparison to the experiments. Solely adding point charges to the propylene model also does not seem sufficient to depict the correct adsorption behavior. In general, the developed polarizable force field performs better than the other force fields. However, for Fe-MOF-74, the propylene uptake at low pressures is substantially overestimated and the force field considering solely polarization agrees better with experiments. The overestimation for the polarizable force field is in agreement with the overprediction observed for the heat of adsorption of propylene in Fe-MOF-74 (cf. Figure 1). It is difficult to provide any conclusive reason for the overestimation of the propylene uptake in Fe-MOF-74 and Fe-MOF-74 seems to be a particularly difficult system to model.

Overall, incorporating polarization and point charges for propylene notably improves the predictions. Considering the adsorption isotherms for all investigated adsorbates, the potential of polarizable force fields for the description of small hydrocarbons is obvious. Adding polarization helps particularly to model the behavior at low uptakes. Without considering polarization the localized electrostatic environment in MOFs with open metal sites cannot be properly described[42,52]. Good agreement between some generic force fields and experimental adsorption isotherms could be a result of error cancellation as heats of adsorption and the binding geometry are modeled inaccurately[63]. However, even explicit polarization cannot provide quantitative predictions. We note that in this study no parameters have been adjusted and therefore, opportunities for further improvements exist. A complete re-parametrization or at least adjustment of the Lennard-Jones parameters, as in our previous work, might be necessary to further enhance the accuracy in predictions[41]. As noted by Franz *et al.*[41], the development of accurate and transferable force fields for hydrocarbons remains to be challenging. Especially, close to the open metal site the energy is low and simulation results may be sensitive to force field parameters that influence the distance and orientation of the adsorbate in this region.

Besides, the Lennard-Jones parameters, the framework charges are an important input in molecular simulation which can influence the location of the adsorbates[41]. To study the influence of varying framework charges, additional simulations are conducted for ethylene in Co-MOF-74 with different point charges. The second set of point charges is computed with the charge equilibration (QEq) method[85,86]. These charges can be computed quickly, but are usually considered to be less accurate than charges from DFT calculations[55]. Figure 8 shows the calculated adsorption isotherm for ethylene in Co-MOF-74 with point charges from the QEq method in comparison to the previously shown results when applying DFT charges at 318 K.

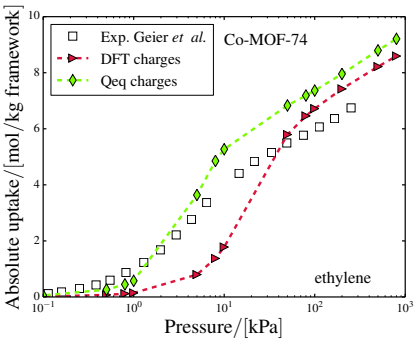

Fig. 8 Adsorption isotherm for ethylene at 318 K predicted with the developed polarizable force field and charges determined via (triangles) DFT calculations, and (diamond) the QEq method.

The calculated adsorption isotherms for ethylene in Co-MOF-74 with QEq charges agrees better with the experiments. This is especially true for lower pressures. The improvement with the QEq charges is rather surprising, since charges from periodic DFT calculations are normally considered to be more accurate[55]. It is important to note that QEq charges did not improve the description of the adsorption for the other investigated frameworks. The large difference in the adsorption isotherms for Co-MOF-74 suggests a large influence of different sets of charges. Such large sensitivities towards assigned point charges have been previously observed for polar molecules in similar systems[87–90]. The previously observed issues could be aggravated by polarizable force fields, since explicit polarization depends on the electric field. Computed adsorption isotherms and heats of adsorption for all considered adsorbates in Co-MOF-74 with charges from the QEq method can be found in the ESI.

To investigate the detailed differences between the two sets of point charges we computed the energy contributions for an ethylene molecule on a grid inside Co-MOF-74. The Lennard-Jones, electrostatic, and polarization energies of ethylene on a grid with a spacing of 0.1 Å inside the pore of Co-MOF-74 are

calculated. For every grid point, 250 approximately uniformly distributed orientations of an ethylene molecule are evaluated. The presented energies represent the Boltzmann average at 318 K of these 250 orientations for every grid point. An energy profile through Co-MOF-74 in z-direction is created via the Widom insertion method[73] to select the plane with the minimum of the Boltzmann average of the total energy (Lennard-Jones, electrostatic, polarization). For this plane the energies are calculated on the grid. Figure 9 shows the Lennard-Jones energy calculated on this plane for ethylene in Co-MOF-74.

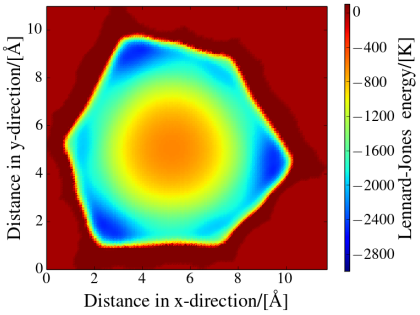

Fig. 9 Lennard-Jones energies evaluated on a grid with 0.1 Å spacing on the minimum energy plane in z-direction for ethylene in Co-MOF-74. Grid points for which the total energy (in units of k_B) is larger than 100 K are represented in dark red.

The two investigated sets of charges do not influence the Lennard-Jones energy surface inside the pore of Co-MOF-74. Therefore, the Lennard-Jones energy surface is identical for the two sets of charges. Grid points where the total energy (in units of k_B) is larger than 100 K are represented in dark red. These grid points are very close or on top of the framework and the repulsion part of the Lennard-Jones potential dominates the energy. The shape of the pore changes along the z-direction and therefore it is not perfectly hexagonal for the shown plane. The open metal sites are located in the 6 corners of the framework. The most favorable adsorption sites are in the vicinity of these sites in the corners of the pore. Three of these open metal sites are located close to the shown plane. Besides the open metal sites, the locations close to the framework are more favorable than the center. With the exception of the repulsive area directly bordering the framework, the Lennard-Jones energy decays as the distance from the surface of the framework increases.

The electrostatic energy calculated with charges from (a) DFT and from (b) the QEq method for the plane with the lowest energy are shown in Figure 10.

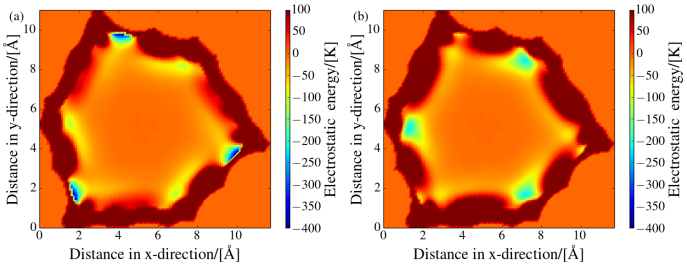

Fig. 10 Comparison between the electrostatic energies for ethylene in Co-MOF-74 on a grid with (a) DFT charges and (b) charges calculated with the QEq method for the plane of minimum energy. Grid points for which the total energy (in units of k_B) is larger than 100 K are represented in dark red.

The energy surface of the electrostatic energy which results from the two different sets of charges varies in the vicinity of the framework. Again, the corners of the pore exhibit the lowest energies. However, the minima for the two sets of charges are located in different corners of the pore. For the DFT charges, the locations of the minima agree with the ones of the Lennard-Jones energy. In contrast to the DFT charges, with the charges from the QEq method, the minima of the static electric energy are predicted to be in the alternating corners. Moreover, the minima of the static electric energy are at lower energies for the DFT charges. Further away from the surface of the framework the static electric energy decays. Therefore, in the center of the pore the influence of static electric interactions is low. For both sets of charges regions of positive energies can be observed close to the framework and between the open metal sites.

In Figure 11, the polarization energy resulting from the electric field created by charges from (a) DFT and from (b) the QEq method is compared for the plane with lowest energy.

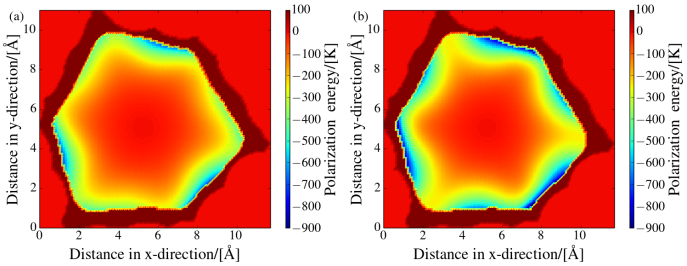

Fig. 11 Comparison between the polarization energies for ethylene in Co-MOF-74 on a grid with (a) DFT charges and (b) charges calculated with the QEq method for the plane of minimum energy. Grid points for which the total energy (in units of k_B) is larger than 100 K are represented in dark red.

The energy surfaces of the polarization energy are similar for both sets of charges, despite the difference in the electrostatic energy. However, close to the framework the concrete values can deviate. Unlike to the electrostatic energy, the polarization energy is always attractive. In addition, the polarization energy declines rapidly and is essentially zero in the center of the pore. This appears reasonable, since polarization is strongly localized. In the vicinity of the surface of the framework the polarization energy is large and it can contribute significantly to the total energy. The

polarization energies can be up to twice as low as the electrostatic energy. It is important to note that the regions of lowest polarization energy border directly on the framework. In the region that is in the close proximity to the framework, the Lennard-Jones energy is already repulsive. Unfortunately, the Lennard-Jones potential was designed rather for computational convenience than for accuracy in the strongly repulsive region[41,70,83]. As a consequence, the quality of the force field for this region might not be sufficient. Rapidly increasing and badly modeled repulsion together with large polarization energies might lead to poor modeling. Such difficulties seem to occur where binding distances are short and interactions are very attractive. An alternative to describe the Lennard-Jones repulsion could be beneficial, e.g., the Buckingham potential[7,62] or a complete re-design of the force field could improve results.

The total energy for both sets of framework charges for the plane of lowest total energy when (left) exclusively electrostatic energies and (right) additional polarization is considered are presented in Figure 12 for (top row) DFT charges and (bottom row) charges determined using the QEq method.

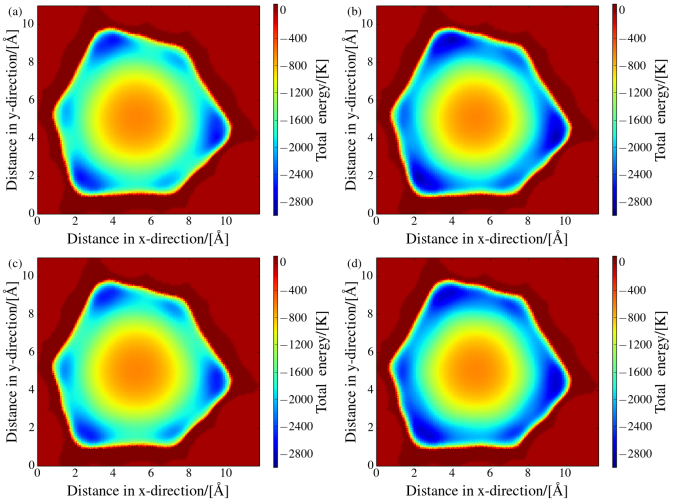

Fig. 12 Comparison between the total energies for ethylene in Co-MOF-74 on a grid (left) without and (right) with explicit consideration of polarization energy. Energies calculated with (a) and (b) DFT charges and (c) and (d) charges calculated with the QEq method for the plane of minimum energy. Grid points for which the total energy (in units of k_B) is larger than 100 K are represented in dark red.

In comparison to solely Lennard-Jones energy (cf. Figure 9), the low energy regions in the corners of the pore are more pronounced when adding point charges to the ethylene model. Especially, the less pronounced local minima in the left, upper right, and lower right corners of the pore are lower in energy (cf. Figure 12 (a) and (c)). If polarizable sites are also added to ethylene, the complete vicinity of the surface of the pore lowers in energy. The difference in energy (in units of k_B) for this region is approximately 300 K. This is a substantial change. Overall, the locations of the minima for both sets of charges agree with the minima of the Lennard-Jones energy and with the location of the open metal sites. The total energies are significantly lower compared to exclusively considering Lennard-Jones energies. It can also be observed that considering polarization in the model may add a large localized contribution to the total energy that can help to describe localized effects. Other non-polarizable classical force fields might fail to describe this behavior[42,52].

The study shows that insights into how polarization contributes to the total energy can help to create a better understanding of adsorption and consequently may be useful to design MOFs with improved capabilities[41]. Interestingly, the different sets of charges do not change the general appearance of the total energy surface. However, for both sets of charges the gradient of total energy close to the open metal sites is very steep which may contribute to the observed sensitivity. The similarity in the total energy surface and the comparison of the adsorption isotherm for ethylene (cf. Figure 8) suggest that differences in the total energy surface lead to large differences in the adsorption. Therefore, an accurate parametrization of the force field parameters may be needed to obtain quantitative agreement between simulations and experiments. The energy surfaces for the maximum energy plane for ethylene show a comparable behavior to the minimum energy plane (can be found in the ESI). Overall, the results show that the choice of charges can have a considerable effect[41,66,67].

5 Conclusions

In this study, the potential of polarizable force fields to calculate the adsorption of small hydrocarbons in Metal-Organic-Frameworks with open metal sites has been investigated. Explicit polarization is considered using the induced dipole model with additional assumptions introduced by Lachet *et al.* [49] to speed up the simulations. Atomic polarizabilities are assigned according to literature[78]. Lennard-Jones interactions and point charges were chosen from standard force fields. To test the predictive potential of polarizable force fields, the force field parameters have not been adjusted. In comparison to generic force fields without considering polarization, the description of the adsorption behavior is significantly improved when including polarization explicitly. Computed heats of adsorption at infinite dilution using the polarizable force field are in reasonable agreement with available experimental data and ab initio predictions. The experimentally observed trend that olefins interact significantly stronger than paraffins was reproduced. Besides, binding geometries follow the experimentally expected trend, .i.e, the double bond of the olefins binds parallel towards the open metal sites, while paraffins point with one side towards the open metal sites. The description of adsorption isotherms for small hydrocarbons is improved as well when including polarization. Even though the agreement for the adsorption isotherm is not perfect, the results are very encouraging. It was shown that polarizable force fields have great potential for the modeling of hydrocarbons in Metal-Organic Frameworks with open metal sites. Polarization can help to describe localized effect close to the surface of porous materials. Good predictions for some adsorbates with standard force fields may be a result of error cancellation, since heats of adsorption and binding energies do not match the expected trends. Simulation results are sensitive towards force field parameters that influence the geometry close to the open metal sites with low total values and steep gradients of total energy. Framework charges are such parameters which

we explored in more detail. Better models may be expected when the description of repulsion is improved. This part is essential for small binding distances as can be observed in MOFs with open metal sites. A complete re-parametrization of the force field and considering explicit polarization from the beginning should enhance the accuracy and lead to force fields with better transferability.

Conflicts of interest

There are no conflicts to declare.

Acknowledgements

This work was sponsored by NWO Exacte Wetenschappen (Physical Sciences) for the use of supercomputer facilities, with financial support from the Nederlandse Organisatie voor Wetenschappelijk Onderzoek (Netherlands Organization for Scientific Research, NWO). TJHV acknowledges NWO-CW for a VICI grant. SC would like to thank for financial support from the Spanish Ministerio de Economía y Competitvidad (CTQ2016-80206-P).

Notes and references

1 B. Liu, B. Smit, F. Rey, S. Valencia and S. Calero, *J. Phys. Chem. C* **2008**, *112*, 2492–2498.

2 E. D. Bloch, W. L. Queen, R. Krishna, J. M. Zadrozny, C. M. Brown and J. R. Long, *Science*, 2012, **335**, 1606–1610.

3 M. M. J. A. Moulijn, M. Michiel, A. E. Van Diepen, *Chemical Process Technology*; John Wiley & Sons, Chichester, 2013.

4 J.-R. Li, R. J. Kuppler and H.-C. Zhou, *Chem. Soc. Rev.*, 2009, **38**, 1477–1504.

5 S. J. Geier, J. A. Mason, E. D. Bloch, W. L. Queen, M. R. Hudson, C. M. Brown and J. R. Long, *Chem. Sci.*, 2013, **4**, 2054–2061.

6 R. B. Eldridge, *Ind. Eng. Chem. Res.*, 1993, **32**, 2208–2212.

7 R. Mercado, B. Vlaisavljevich, L.-C. Lin, K. Lee, Y. Lee, J. A. Mason, D. J. Xiao, M. I. Gonzalez, M. T. Kapelewski, J. B. Neaton and B. Smit, *J. Phys. Chem. C*, 2016, **120**, 12590–12604.

8 Y. He, R. Krishna and B. Chen, *Energy Environ. Sci.*, 2012, **5**, 9107–9120.

9 J. Gascon, W. Blom, A. van Miltenburg, A. Ferreira, R. Berger and F. Kapteijn, *Micropor. Mesopor. Mat.*, 2008, **115**, 585–593.

10 J. Van den Bergh, C. Gücüyener, E. A. Pidko, E. J. M. Hensen, J. Gascon and F. Kapteijn, *Chem. Eur. J.*, 2011, **17**, 8832–8840.

11 Y.-S. Bae, C. Y. Lee, K. C. Kim, O. K. Farha, P. Nickias, J. T. Hupp, S. T. Nguyen and R. Q. Snurr, *Angew. Chem. Int. Ed.*, 2012, **51**, 1857–1860.

12 J. L. Rowsell and O. M. Yaghi, *Micropor. Mesopor. Mat.*, 2004, **73**, 3–14.

13 Z. R. Herm, J. A. Swisher, B. Smit, R. Krishna and J. R. Long, *J. Am. Chem. Soc.*, 2011, **133**, 5664–5667.

14 P. D. Dietzel, V. Besikiotis and R. Blom, *J. Mater. Chem.*, 2009, **19**, 7362–7370.

15 A. Ö. Yazaydin, R. Q. Snurr, T.-H. Park, K. Koh, J. Liu, M. D. LeVan, A. I. Benin, P. Jakubczak, M. Lanuza, D. B. Galloway, J. J. Low and R. R. Willis, *J. Am. Chem. Soc.*, 2009, **131**, 18198–18199.

16 R. Krishna and J. M. van Baten, *J. Membrane Sci.*, 2011, **377**, 249–260.

17 A. L. Dzubak, L.-C. Lin, J. Kim, J. A. Swisher, R. Poloni, S. N. Maximoff, B. Smit and L. Gagliardi, *Nat. Chem.*, 2012, **4**, 810–816.

18 L.-C. Lin, K. Lee, L. Gagliardi, J. B. Neaton and B. Smit, *J. Chem. Theory Comput.*, 2014, **10**, 1477–1488.

19 K. Lee, W. C. I. III, A. L. Dzubak, P. Verma, S. J. Stoneburner, L.-C. Lin, J. D. Howe, E. D. Bloch, D. A. Reed, M. R. Hudson, C. M. Brown, J. R. Long, J. B. Neaton, B. Smit, C. J. Cramer, D. G. Truhlar and L. Gagliardi, *J. Am. Chem. Soc.*, 2014, **136**, 698–704.

20 W. L. Queen, M. R. Hudson, E. D. Bloch, J. A. Mason, M. I. Gonzalez, J. S. Lee, D. Gygi, J. D. Howe, K. Lee, T. A. Darwish, M. James, V. K. Peterson, S. J. Teat, B. Smit, J. B. Neaton, J. R. Long and C. M. Brown, *Chem. Sci.*, 2014, **5**, 4569–4581.

21 N. L. Rosi, J. Kim, M. Eddaoudi, B. Chen, M. O'Keeffe and O. M. Yaghi, *J. Am. Chem. Soc.*, 2005, **127**, 1504–1518.

22 P. D. C. Dietzel, Y. Morita, R. Blom and H. Fjellvåg, *Angew. Chem.*, 2005, **117**, 6512–6516.

23 P. D. C. Dietzel, B. Panella, M. Hirscher, R. Blom and H. Fjellvag, *Chem. Commun.*, 2006, 959–961.

24 W. Zhou, H. Wu and T. Yildirim, *J. Phys. Chem. C*, 2008, **112**, 8132–8135.

25 S. Bhattacharjee, J.-S. Choi, S.-T. Yang, S. B. Choi, J. Kim and W.-S. Ahn, *J. Nanosci. Nanotechno.*, 2010, **10**, 135–141.

26 P. D. C. Dietzel, R. Blom and H. Fjellvåg, *Eur. J. Inorg. Chem.*, 2008, **2008**, 3624–3632.

27 R. Sanz, F. Martinez, G. Orcajo, L. Wojtas and D. Briones, *Dalton T.*, 2013, **42**, 2392–2398.

28 A. F. Ferreira, J. C. Santos, M. G. Plaza, N. Lamia, J. M. Loureiro and A. E. Rodrigues, *Chem. Eng. J.*, 2011, **167**, 1–12.

29 K. Li, D. H. Olson, J. Seidel, T. J. Emge, H. Gong, H. Zeng and J. Li, *J. Am. Chem. Soc.*, 2009, **131**, 10368–10369.

30 J. Heinen, N. C. Burtch, K. S. Walton, C. Fonseca Guerra and D. Dubbeldam, *Chem. Eur. J.*, 2016, **22**, 18045–18050.

31 P. Mishra, S. Edubilli, B. Mandal and S. Gumma, *J. Phys. Chem. C*, 2014, **118**, 6847–6855.

32 P. Verma, X. F. Xu and D. G. Truhlar, *J. Phys. Chem. C*, 2013, **117**, 12648–12660.

33 U. Böhme, B. Barth, C. Paula, A. Kuhnt, W. Schwieger, A. Mundstock, J. Caro and M. Hartmann, *Langmuir*, 2013, **29**, 8592–8600.

34 H. Wu, W. Zhou and T. Yildirim, *J. Am. Chem. Soc.*, 2009, **131**, 4995–5000.

35 E. D. Bloch, L. J. Murray, W. L. Queen, S. Chavan, S. N. Maximoff, J. P. Bigi, R. Krishna, V. K. Peterson, F. Grandjean, G. J. Long, B. Smit, S. Bordiga, C. M. Brown and J. R. Long, *J. Am. Chem. Soc.*, 2011, **133**, 14814–14822.

36 J. A. Mason, K. Sumida, Z. R. Herm, R. Krishna and J. R. Long, *Energy Environ. Sci.*, 2011, **4**, 3030–3040.

37 Z. Bao, S. Alnemrat, L. Yu, I. Vasiliev, Q. Ren, X. Lu and S. Deng, *Langmuir*, 2011, **27**, 13554–13562.

38 K. Lee, J. D. Howe, L.-C. Lin, B. Smit and J. B. Neaton, *Chem. Mater.*, 2015, **27**, 668–678.

39 Frenkel, D.; Smit, B. *Understanding Molecular Simulation (Second Edition)*; Academic Press: San Diego, 2002.

40 J. G. McDaniel, K. Yu and J. Schmidt, *J. Phys. Chem. C*, 2012, **116**, 1892–1903.

41 D. M. Franz, Z. E. Dyott, K. A. Forrest, A. Hogan, T. Pham and B. Space, *Phys. Chem. Chem. Phys.*, 2018, **20**, 1761–1777.

42 K. A. Forrest, T. Pham, K. McLaughlin, J. L. Belof, A. C. Stern, M. J. Zaworotko and B. Space, *J. Phys. Chem. C*, 2012, **116**, 15538–15549.

43 M. Jorge, M. Fischer, J. R. B. Gomes, C. Siquet, J. C. Santos and A. E. Rodrigues, *Ind. Eng. Chem. Res.*, 2014, **53**, 15475–15487.

44 A. Luna-Triguero, J. M. Vicent-Luna, T. M. Becker, T. J. H. Vlugt, D. Dubbeldam, P. Gómez-Álvarez and S. Calero, *ChemistrySelect*, 2017, **2**, 665–672.

45 L. Chen, L. Grajciar, P. Nachtigall and T. Düren, *J. Phys. Chem. C*, 2011, **115**, 23074–23080.

46 M. Fischer, J. R. B. Gomes, M. Fröba and M. Jorge, *Langmuir*, 2012, **28**, 8537–8549.

47 J. J. Gutiérrez-Sevillano, D. Dubbeldam, F. Rey, S. Valencia, M. Palomino, A. Martín-Calvo and S. Calero, *J. Phys. Chem. C*, 2010, **114**, 14907–14914.

48 F. D. Lahoz-Martín, S. Calero, J. J. Gutiérrez-Sevillano and A. Martin-Calvo, *Microporous and Mesoporous Materials*, 2017, **248**, 40–45.

49 V. Lachet, A. Boutin, B. Tavitian and A. Fuchs, *J. Phys. Chem. B*, 1998, **102**, 9224–9233.

50 J. Kim, L.-C. Lin, R. L. Martin, J. A. Swisher, M. Haranczyk and B. Smit, *Langmuir*, 2012, **28**, 11914–11919.

51 C. D. Wick, M. G. Martin and J. I. Siepmann, *J. Phys. Chem. B*, 2000, **104**, 8008–8016.

52 J. L. Belof, A. C. Stern and B. Space, *J. Chem. Theory Comput.*, 2008, **4**, 1332–1337.

53 T. Pham, K. A. Forrest, R. Banerjee, G. Orcajo, J. Eckert and B. Space, *J. Phys. Chem. C*, 2015, **119**, 1078–1090.

54 M. G. Martin, B. Chen and J. I. Siepmann, *J. Chem. Phys.*, 1998, **108**, 3383–3385.

55 S. Hamad, S. R. Balestra, R. Bueno-Perez, S. Calero and A. R. Ruiz-Salvador, *J. Solid State Chem.*, 2015, **223**, 144 – 151.

56 Lucas, K. *Molecular Models for Fluids*; Cambridge University Press, 2007.

57 M. S. Shah, J. I. Siepmann and M. Tsapatsis, *AIChE J.*, 2017, **63**, 5098–5110.

58 Rick, S. W.; Stuart, S. J. Potentials and Algorithms for Incorporating Polarizability in Computer Simulations. In *Reviews in Computational Chemistry (First Edition)*; John Wiley & Sons, Inc.: Hoboken, 2003; Vol. 18, pp 89–146.

59 Antila, H. S.; Salonen, E. Polarizable Force Fields. In *Biomolecular Simulations (First Edition)*; Humana Press: Clifton, 2013; pp 215–241.

60 J. Wang, P. Cieplak, J. Li, T. Hou, R. Luo and Y. Duan, *J. Phys. Chem. B*, 2011, **115**, 3091–3099.

61 T. M. Becker, D. Dubbeldam, L.-C. Lin and T. J. H. Vlugt, *J. Comput. Sci.* **2016**, *15*, 86–94.

62 J. G. McDaniel and J. R. Schmidt, *J. Phys. Chem. C*, 2012, **116**, 14031–14039.

63 J. G. McDaniel, S. Li, E. Tylianakis, R. Q. Snurr and J. R. Schmidt, *J. Phys. Chem. C*, 2015, **119**, 3143–3152.

64 J. L. Belof, A. C. Stern, M. Eddaoudi and B. Space, *J. Am. Chem. Soc.*, 2007, **129**, 15202–15210.

65 T. Pham, K. A. Forrest, A. Hogan, K. McLaughlin, J. L. Belof, J. Eckert and B. Space, *J. Mater. Chem. A*, 2014, **2**, 2088–2100.

66 T. Pham, K. A. Forrest, W.-Y. Gao, S. Ma and B. Space, *ChemPhysChem*, **16**, 3170–3179.

67 T. Pham, K. A. Forrest, D. M. Franz, Z. Guo, B. Chen and B. Space, *Phys. Chem. Chem. Phys.*, 2017, **19**, 18587–18602.

68 T. M. Becker, J. Heinen, D. Dubbeldam, L.-C. Lin and T. J. H. Vlugt, *J. Phys. Chem. C*, 2017, **121**, 4659–4673.

69 T. M. Becker, L.-C. Lin, D. Dubbeldam and T. J. H. Vlugt, *J. Phys. Chem. C*, 2018, **122**, 24488–24498.

70 H. Fang, H. Demir, P. Kamakoti and D. S. Sholl, *J. Mater. Chem. A*, 2014, **2**, 274–291.

71 D. Dubbeldam, S. Calero, D. E. Ellis and R. Q. Snurr, *Mol. Simulat.* **2016**, *30*, 81–101.

72 D. Dubbeldam, A. Torres-Knoop and K. S. Walton, *Mol. Simulat.* **2013**, *39*, 1253–1292.

73 T. J. H. Vlugt, E. García-Pérez, D. Dubbeldam, S. Ban and S. Calero, *J. Chem. Theory Comput.*, 2008, **4**, 1107–1118.

74 S. L. Mayo, B. D. Olafson and W. A. Goddard, *J. Phys. Chem.*, 1990, **94**, 8897–8909.

75 A. K. Rappe, C. J. Casewit, K. S. Colwell, W. A. Goddard and W. M. Skiff, *J. Am. Chem. Soc.*, 1992, **114**, 10024–10035.

76 T. Schnabel, J. Vrabec and H. Hasse, *J. Mol. Liq.*, 2007, **135**, 170 – 178.

77 Allen, M. P.; Tildesley, D. J. *Computer Simulation of Liquids (Second Edition)*; Oxford University Press, 2017.

78 J. M. Stout and C. E. Dykstra, *J. Am. Chem. Soc.*, 1995, **117**, 5127–5132.

79 D.-Y. Peng and D. B. Robinson, *Ind. Eng. Chem. Fund.*, 1976, **15**, 59–64.

80 Perry, R. H.; Green, D. W.; Maloney, J. O.; Abbott, M. M.; Ambler, C. M.; Amero, R. C. *Perry's Chemical Engineers' Handbook (Vol. 7)*; McGraw-Hill New York, 1997.

81 J. Park, J. D. Howe and D. S. Sholl, *Chem. Mater.*, 2017, **29**, 10487 – 10495.

82 Dubbeldam, D.; Walton, K. S. On the Application of Classical Molecular Simulations of Adsorption in Metal-Organic Frameworks. In *Metal-Organic Frameworks: Materials Modeling towards Engineering Applications (First Edition)*; CRC Press: Boca Raton, 2015; pp 53-112.

83 E. Haldoupis, J. Borycz, H. Shi, K. D. Vogiatzis, P. Bai, W. L. Queen, L. Gagliardi and J. I. Siepmann, *J. Phys. Chem. C*, 2015, **119**, 16058–16071.

84 J. Borycz, D. Tiana, E. Haldoupis, J. C. Sung, O. K. Farha, J. I. Siepmann and L. Gagliardi, *J. Phys. Chem. C*, 2016, **120**, 12819–12830.

85 A. K. Rappe and W. A. Goddard, *J. Phys. Chem.*, 1991, **95**, 3358–3363.

86 E. Haldoupis, S. Nair and D. S. Sholl, *J. Am. Chem. Soc.*, 2012, **134**, 4313–4323.

87 J. M. Castillo, T. J. H. Vlugt and S. Calero, *J. Phys. Chem. C*, 2008, **112**, 15934–15939.

88 R. Babarao and J. Jiang, *J. Phys. Chem. C*, 2009, **113**, 18287–18291.

89 Y. F. Chen, R. Babarao, S. I. Sandler and J. W. Jiang, *Langmuir*, 2010, **26**, 8743–8750.

90 J. J. Gutierrez-Sevillano, A. Caro-Perez, D. Dubbeldam and S. Calero, *Phys. Chem. Chem. Phys.*, 2011, **13**, 20453–20460.

Electronic Supplementary Information: Potential of Polarizable Force Fields for Predicting the Separation Performance of Small Hydrocarbons in M-MOF-74

Tim M. Becker,[†] Azahara Luna-Triguero,[‡] Jose Manuel Vicent-Luna,[‡] Li-Chiang Lin,[¶] David Dubbeldam,[†,§] Sofia Calero,[‡] and Thijs J. H. Vlugt[*,†]

Engineering Thermodynamics, Process & Energy Department, Faculty of Mechanical, Maritime and Materials Engineering, Delft University of Technology, Leeghwaterstraat 39, 2628CB Delft, The Netherlands, Department of Physical, Chemical and Natural Systems, Universidad Pablo de Olavide, Ctra. Utrera km 1. ES-41013, Seville, Spain, William G. Lowrie Department of Chemical and Biomolecular Engineering, The Ohio State University, 151 W. Woodruff Ave., Columbus, OH 43210, United States, and Van't Hoff Institute for Molecular Sciences, University of Amsterdam, Science Park 904, 1098XH Amsterdam, The Netherlands

E-mail: t.j.h.vlugt@tudelft.nl

[*]To whom correspondence should be addressed
[†]Delft University of Technology
[‡]Universidad Pablo de Olavide
[¶]The Ohio State University
[§]University of Amsterdam

The Electronic Supplementary Information consists of 6 parts. The first part summarizes all force field parameters adopted in this study. Tables 1 to 4 provide the parameters for the M-MOF-74 frameworks. Tables 5 to 12 summarize the force field parameters of the adsorbates. In Figure 1, a representation of all considered interaction sites of M-MOF-74 with labels is provided. In the second part, a schematic view of the binding geometry for C3 hydrocarbons is shown (Figure 2). Subsequently, the binding geometries for all systems are provided (Figures 3 to 6). Next, adsorption isotherms calculated using the force field of Liu *et al.*[1] with the addition of explicit polarization are shown. In part 5, the details of the force field (Table 13) and the results of the calculations of Co-MOF-74 using charges determined via the charge equilibration (QEq) method are provided (Figures 11 to 14). Finally, the energy surfaces determined for the plane of maximum energy are shown in Figures 15 to 18.

Force field parameters

Table 1: Force field parameters for Co-MOF-74. The charges are taken from previous studies[2–4]. The framework is considered to be rigid.

#	Atom type	$\varepsilon\ /k_B$ [K]	σ [Å]	Partial charge [e]
1	Co	7.045	2.56	1.189
2	O1	47.86	3.473	−0.720
3	O2	47.86	3.473	−0.673
4	O3	47.86	3.473	−0.725
5	C1	48.19	3.033	0.846
6	C2	48.19	3.033	−0.308
7	C3	48.19	3.033	0.391
8	C4	48.19	3.033	−0.177
9	H	7.65	2.846	0.177

Table 2: Force field parameters for Fe-MOF-74. The charges are taken from previous studies[2–4]. The framework is considered to be rigid.

#	Atom type	$\varepsilon\ /k_B$ [K]	σ [Å]	Partial charge [e]
1	Fe	6.54	2.59	1.288
2	O1	47.86	3.473	−0.753
3	O2	47.86	3.473	−0.707
4	O3	47.86	3.473	−0.794
5	C1	48.19	3.033	0.870
6	C2	48.19	3.033	−0.337
7	C3	48.19	3.033	0.432
8	C4	48.19	3.033	−0.195
9	H	7.65	2.846	0.196

Table 3: Force field parameters for Mn-MOF-74. The charges are taken from previous studies[2–4]. The framework is considered to be rigid.

#	Atom type	$\varepsilon\ /k_B$ [K]	σ [Å]	Partial charge [e]
1	Mn	6.54	2.64	1.343
2	O1	47.86	3.473	−0.754
3	O2	47.86	3.473	−0.717
4	O3	47.86	3.473	−0.806
5	C1	48.19	3.033	0.850
6	C2	48.19	3.033	−0.296
7	C3	48.19	3.033	0.396
8	C4	48.19	3.033	−0.203
9	H	7.65	2.846	0.187

Table 4: Force field parameters for Ni-MOF-74. The charges are taken from previous studies[2–4]. The framework is considered to be rigid.

#	Atom type	$\varepsilon\ /k_B$ [K]	σ [Å]	Partial charge [e]
1	Ni	7.55	2.52	1.298
2	O1	47.86	3.473	−0.789
3	O2	47.86	3.473	−0.696
4	O3	47.86	3.473	−0.785
5	C1	48.19	3.033	0.895
6	C2	48.19	3.033	−0.349
7	C3	48.19	3.033	0.418
8	C4	48.19	3.033	−0.173
9	H	7.65	2.846	0.181

Table 5: Force field parameters and atomic polarizabilities for ethane. Atomic polarizabilities are taken from Stout and Dykstra[5].

#	Atom type	$\varepsilon\ /k_B$ [K]	σ [Å]	α [Å^3]	Partial charge [e]
TraPPE[6]	CH3	98.0	3.75	-	-
Liu[1]	CH3	108.0	3.76	-	-
Pol. force field	CH3	98.0	3.75	1.874	-

Table 6: Geometries used for ethane. Bending potential according to $U^{\text{bend}} = \frac{1}{2} \cdot k_\circ \cdot (r - r_\circ)^2$

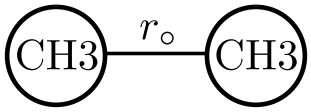

#	$r_\circ$ / [Å]	$k_\circ/\boldsymbol{k}_B$ [K/Å^2]
TraPPE	1.54	rigid
Liu	1.54	96500
Pol. force field	1.54	rigid

Table 7: Force field parameters and atomic polarizabilities for ethylene. Atomic polarizabilities are taken from Stout and Dykstra[5].

#	Atom type	$\varepsilon\ /k_B$ [K]	σ [Å]	α [Å^3]	Partial charge [e]
TraPPE[6]	CH2	85.0	3.675	-	-
Liu[1]	CH2	93.0	3.685	-	-
Pol. force field	CH2	93.0	3.722	1.959	0.73
Pol. force field	dummy	0.0	0.0	-	−1.46
No charges	CH2	85.0	3.675	1.959	-
No polarization[7]	CH2	93.0	3.722	-	0.73
No polarization[7]	dummy	0.0	0.0	-	−1.46

Table 8: Geometries used for ethylene. Bending potential according to $U^{\text{bend}} = \frac{1}{2} \cdot k_\circ \cdot (r - r_\circ)^2$

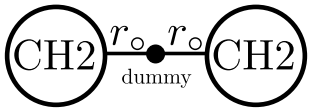

#	$r_\circ$ / [Å]	$k_\circ/\boldsymbol{k}_B$ / [K/Å^2]
TraPPE	0.6665	rigid
Liu	0.6665	96500
Pol. force field	0.6695	rigid
No charges	0.6665	rigid
No polarization	0.6695	rigid

Table 9: Force field parameters and atomic polarizabilities for propane. Atomic polarizabilities are taken from Stout and Dykstra[5].

#	Atom type	$\varepsilon\ /k_B$ / [K]	σ [Å]	α [Å^3]	Partial charge [e]
TraPPE[6]	CH3	98.0	3.75	-	-
TraPPE[6]	CH2	46.0	3.95	-	-
Liu[1]	CH3	108.0	3.76	-	-
Liu[1]	CH2	56.0	3.96	-	-
Pol. force field	CH3	98.0	3.75	1.874	-
Pol. force field	CH2	46.0	3.95	1.874	-

Table 10: Geometries used for propane. Bond potential according to $U^{\text{bond}} = \frac{1}{2} \cdot k_\circ \cdot (r - r_\circ)^2$ and bending according to $U^{\text{bend}} = \frac{1}{2} \cdot k_\theta \cdot (\theta - \theta_\circ)^2$.

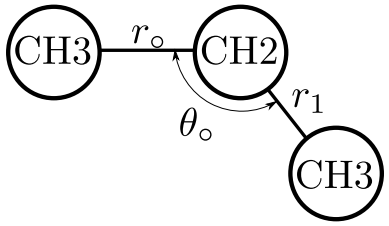

#	$r_\circ$ / [Å]	$k_\circ/\boldsymbol{k}_B$ [K/Å^2]	r_1 / [Å]	$p_1/\boldsymbol{k}_B$ [K/Å^2]	$\theta_\circ$ / [°]	$k_\theta/\boldsymbol{k}_B$ [K/rad^2]
TraPPE	1.54	rigid	1.54	rigid	114	62500
Liu	1.54	96500	1.54	96500	114	62500
Pol. force field	1.54	rigid	1.54	rigid	114	62500

Table 11: Force field parameters and atomic polarizabilities for propylene. Atomic polarizabilities are taken from Stout and Dykstra[5].

#	Atom type	$\varepsilon\ /k_B$ [K]	σ [Å]	α [Å^3]	Partial charge [e]
TraPPE[6]	CH3	98.0	3.75	-	-
TraPPE[6]	CH	47.0	3.73	-	-
TraPPE[6]	CH2	85.0	3.675	-	-
Liu[1]	CH3	108.0	3.76	-	-
Liu[1]	CH	53.0	3.74	-	-
Liu[1]	CH2	93.0	3.685	-	-
Pol. force field	CH3	108.0	3.76	1.874	-
Pol. force field	CH	53.0	3.74	1.959	0.87
Pol. force field	CH2	93.0	3.685	1.959	0.87
Pol. force field	dummy	0.0	0.0	-	−1.74
No charges	CH3	98.0	3.75	1.874	-
No charges	CH	47.0	3.73	1.959	-
No charges	CH2	85.0	3.675	1.959	-
No polarization[8]	CH3	108.0	3.76	-	-
No polarization[8]	CH	53.0	3.74	-	0.87
No polarization[8]	CH2	93.0	3.685	-	0.87
No polarization[8]	dummy	0.0	0.0	-	−1.74

Table 12: Geometries used for propylene. Bond potential according to $U^{\text{bond}} = \frac{1}{2} \cdot k_\circ \cdot (r - r_\circ)^2$ and bending according to $U^{\text{bend}} = \frac{1}{2} \cdot k_\theta \cdot (\theta - \theta_\circ)^2$.

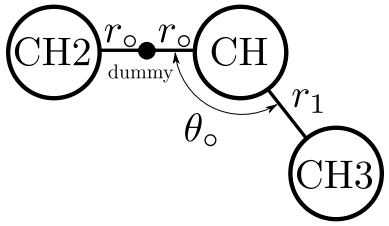

#	$r_\circ$ / [Å]	$k_\circ/\boldsymbol{k}_B$ [K/Å^2]	r_1 / [Å]	$p_1/\boldsymbol{k}_B$ [K/Å^2]	$\theta_\circ$ / [°]	$k_\theta/\boldsymbol{k}_B$ [K/rad^2]
TraPPE	0.665	rigid	1.54	rigid	119.7	70420
Liu	0.665	96500	1.54	96500	119.7	70420
Pol. force field	0.704	rigid	1.54	96500	119.7	70420
No charges	0.665	rigid	1.54	rigid	119.7	70420
No polarization	0.704	rigid	1.54	96500	119.7	70420

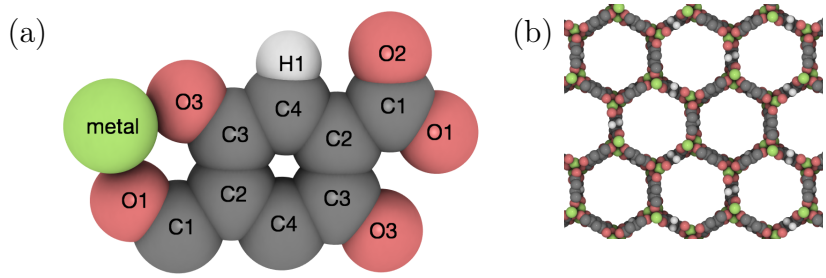

Figure 1: (a) Labeling of the interaction sites and (b) the framework of M-MOF-74. Metal, carbon, oxygen, and hydrogen are depicted in green, gray, red, and white, respectively.

Representation of binding geometry for C3 hydrocarbons

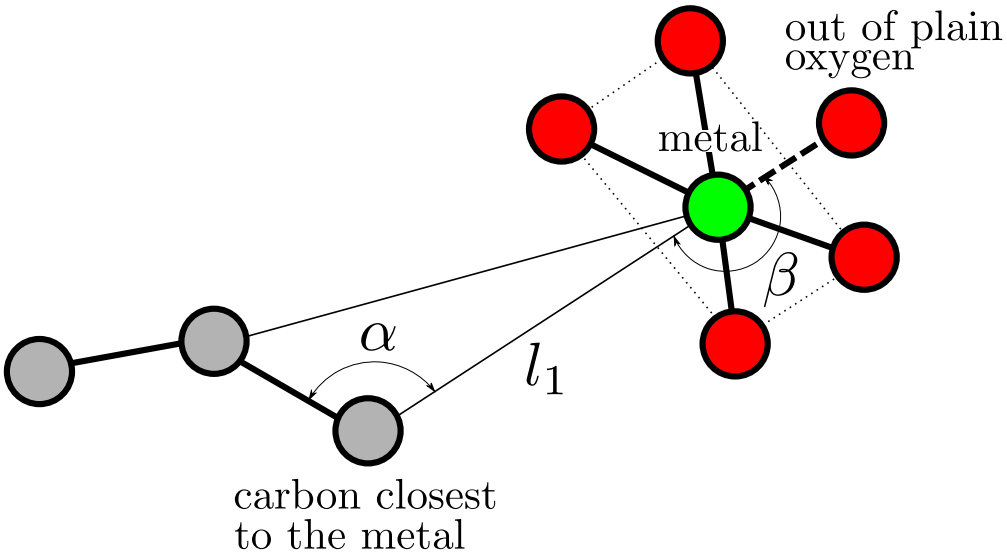

Figure 2: Schematic representation of the binding geometry for C3 hydrocarbons within M-MOF-74. Carbon atoms, the metal atom, and oxygen atoms are colored in grey, green, and red, respectively.

Binding Geometries

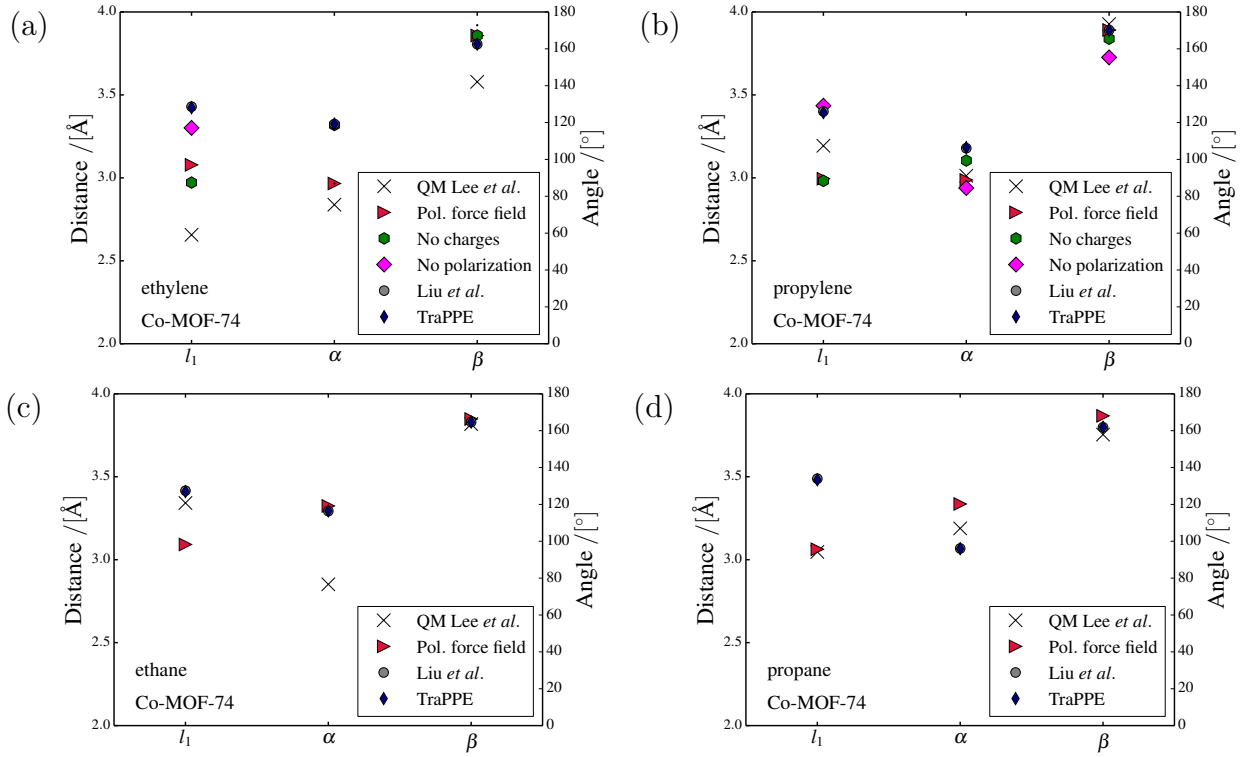

Figure 3: Summary of parameters to describe the binding geometry in Co-MOF-74. Comparison between several classical force fields and the DFT results of Lee *et al.*[3]. Parameters are defined according to Figure 2 of the main text.

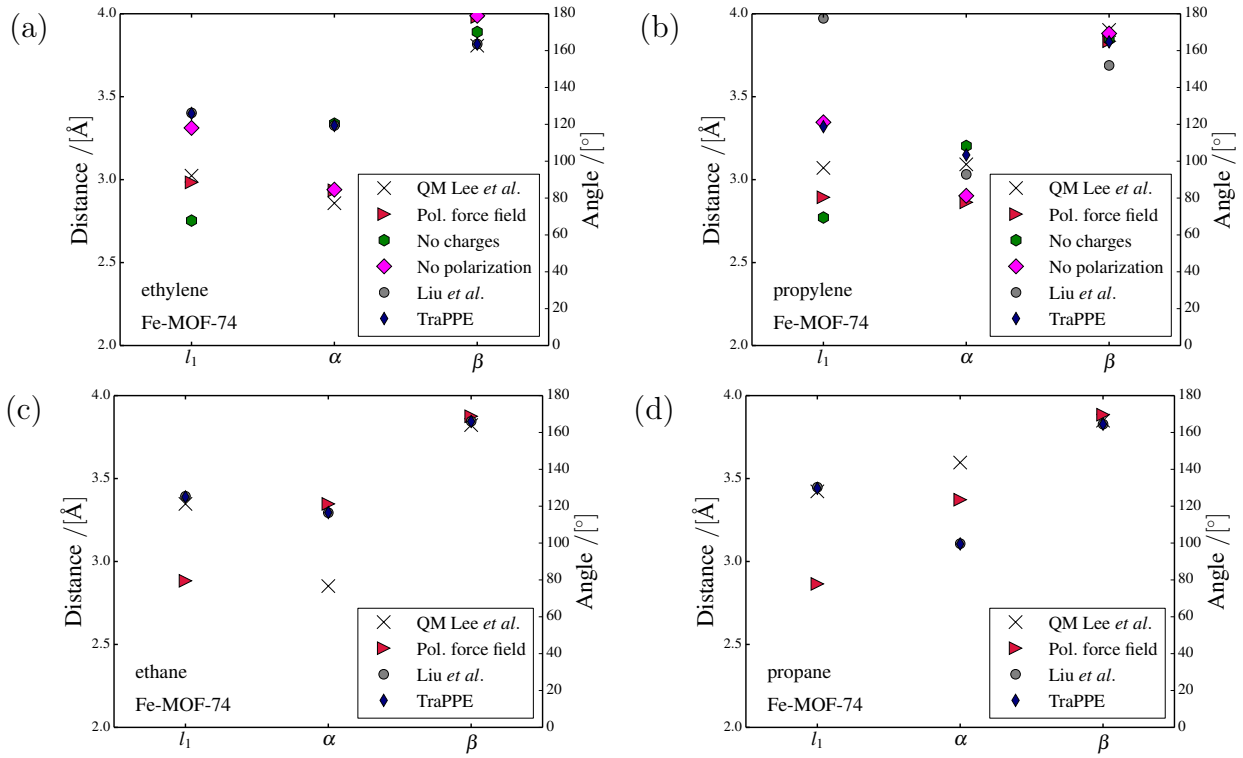

Figure 4: Summary of parameters to describe the binding geometry in Fe-MOF-74. Comparison between several classical force fields and the DFT results of Lee *et al.*[3]. Parameters are defined according to Figure 2 of the main text.

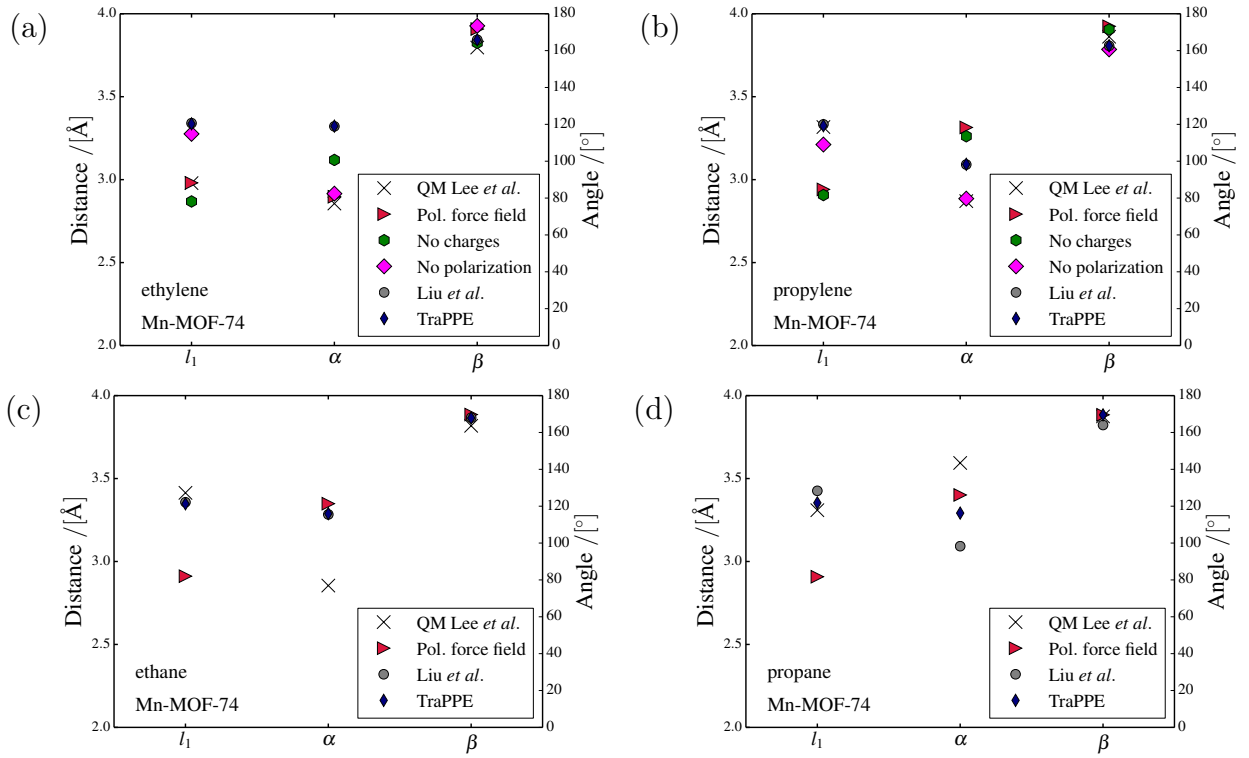

Figure 5: Summary of parameters to describe the binding geometry in Mn-MOF-74. Comparison between several classical force fields and the DFT results of Lee *et al.*[3]. Parameters are defined according to Figure 2 of the main text.

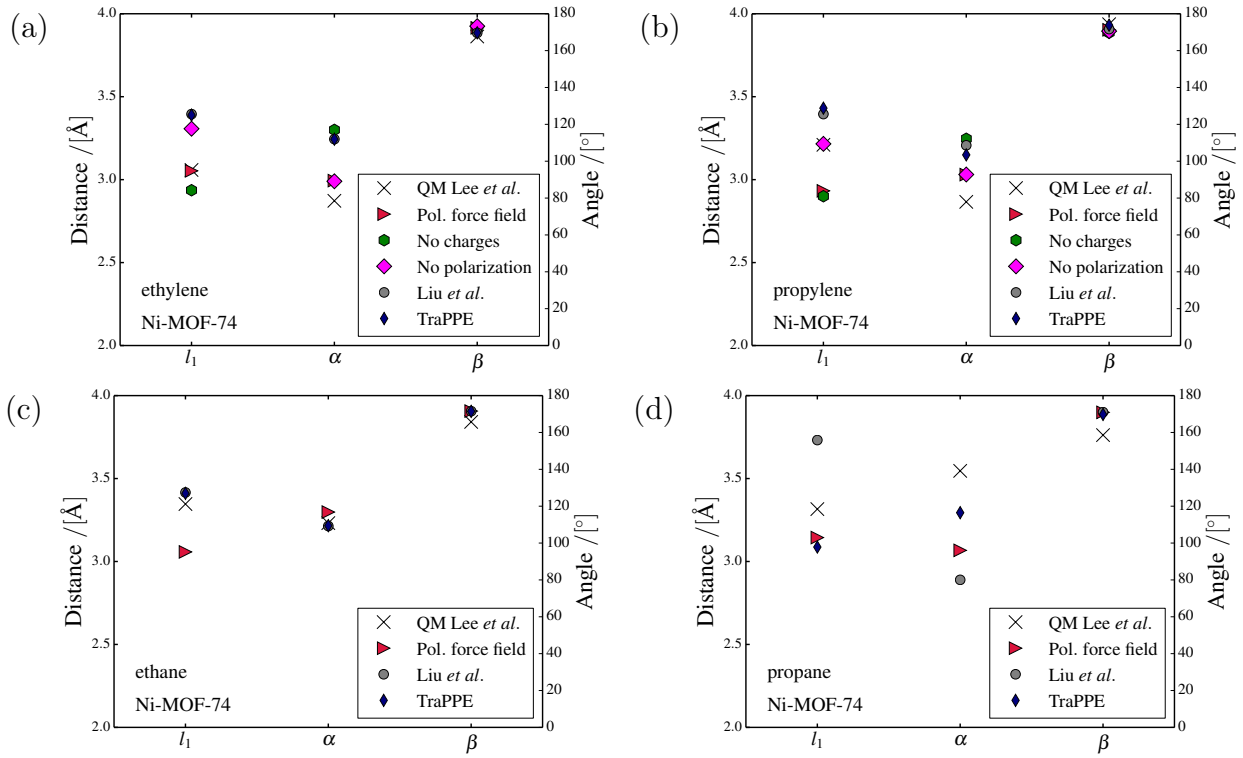

Figure 6: Summary of parameters to describe the binding geometry in Ni-MOF-74. Comparison between several classical force fields and the DFT results of Lee *et al.*[3]. Parameters are defined according to Figure 2 of the main text.

Adsorption isotherms with the force field of Liu *et al.*[1] and additional polarization

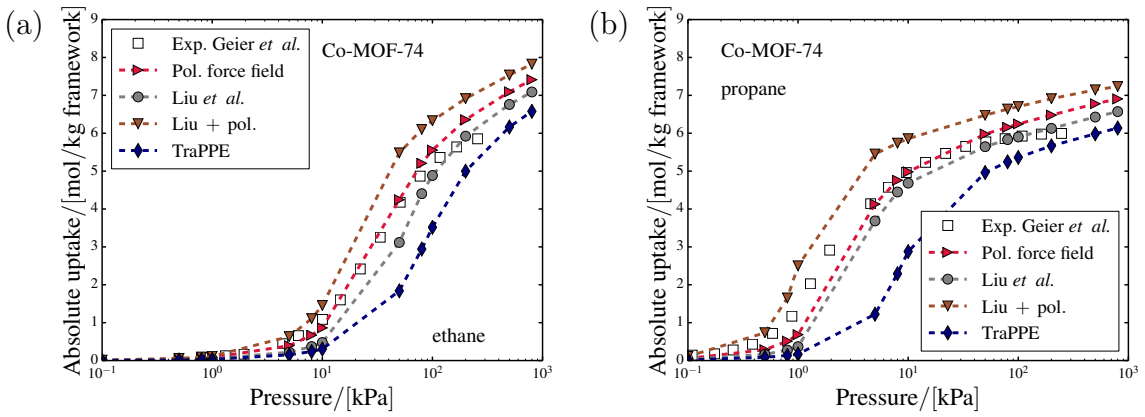

Figure 7: Adsorption isotherm for (a) ethane and (b) propane in Co-MOF-74 at 318 K predicted with the force field of Liu *et al.*[1] with and without adding explicit polarization. Comparison with the polarizable force field, the TraPPE force field[6], and the experimental values of Geier *et al.*[9].

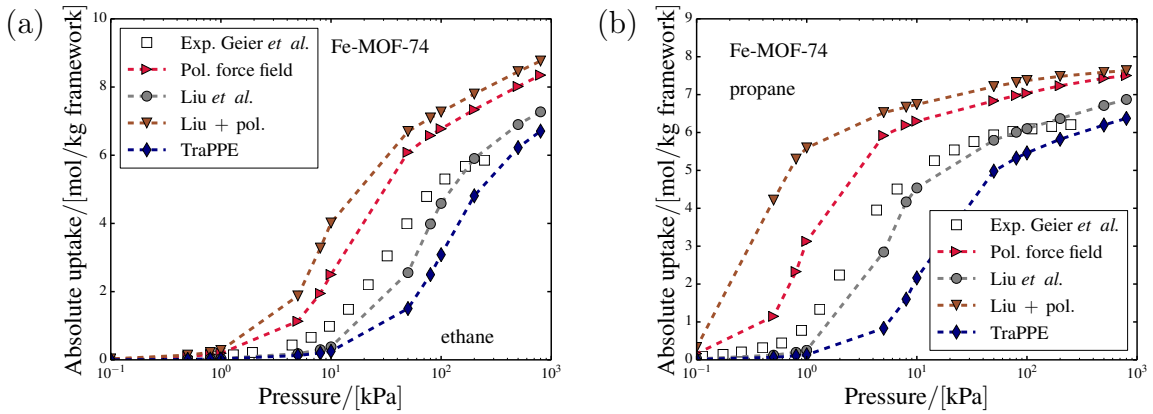

Figure 8: Adsorption isotherm for (a) ethane and (b) propane in Fe-MOF-74 at 318 K predicted with the force field of Liu *et al.*[1] with and without adding explicit polarization. Comparison with the polarizable force field, the TraPPE force field[6], and the experimental values of Geier *et al.*[9].

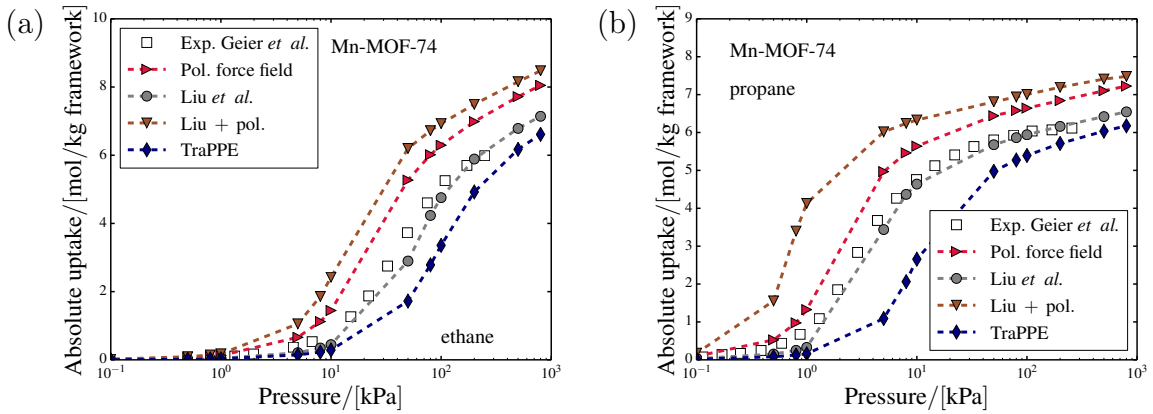

Figure 9: Adsorption isotherm for (a) ethane and (b) propane in Mn-MOF-74 at 318 K predicted with the force field of Liu *et al.*[1] with and without adding explicit polarization. Comparison with the polarizable force field, the TraPPE force field[6], and the experimental values of Geier *et al.*[9].

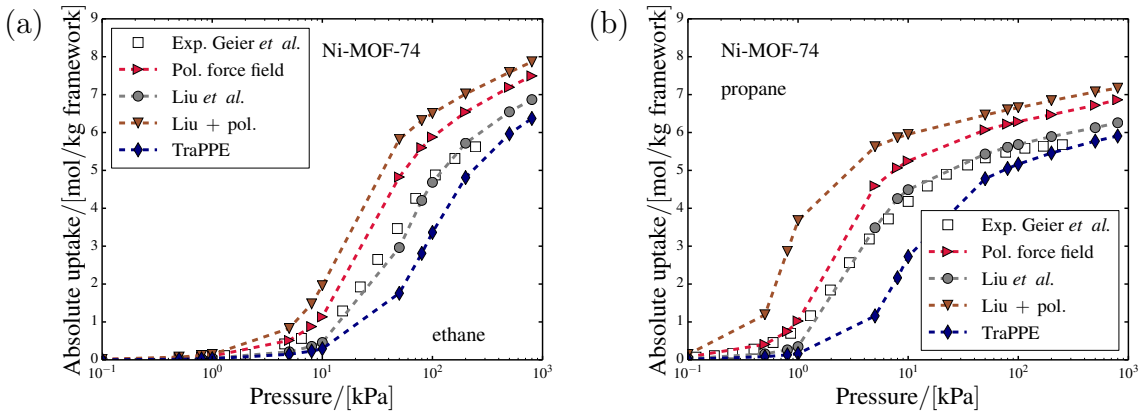

Figure 10: Adsorption isotherm for (a) ethane and (b) propane in Ni-MOF-74 at 318 K predicted with the force field of Liu *et al.*[1] with and without adding explicit polarization. Comparison with the polarizable force field, the TraPPE force field[6], and the experimental values of Geier *et al.*[9].

Force field parameters, heats of adsorption, and adsorption isotherms for Co-MOF-74 with QEq charges

Table 13: Force field parameters for Co-MOF-74 with charges calculated with the charge equilibration (QEq) method[10,11]. The framework is considered to be rigid.

#	Atom type	$\varepsilon\ /k_B$ [K]	σ [Å]	Partial charge [e]
1	Co	7.045	2.56	1.162
2	O1	47.86	3.473	−0.473
3	O2	47.86	3.473	−0.531
4	O3	47.86	3.473	−0.585
5	C1	48.19	3.033	0.423
6	C2	48.19	3.033	−0.180
7	C3	48.19	3.033	0.209
8	C4	48.19	3.033	−0.108
9	H	7.65	2.846	0.083

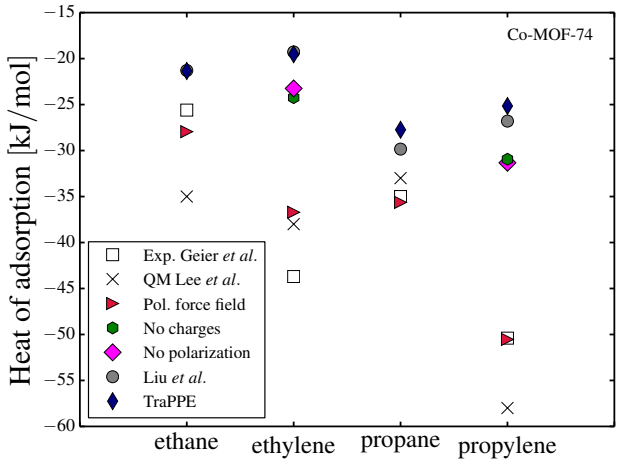

Figure 11: Heats of adsorption for Co-MOF-74 at infinite dilution calculated at 318 K with various force fields. The computational results are compared to DFT binding energies from Lee *et al.*[3] and heats of adsorption predicted via the Clausius-Clapeyron equation by Geier *et al.*[9].

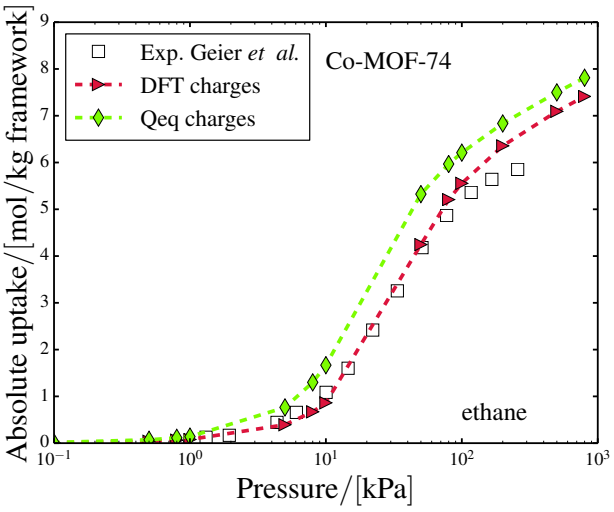

Figure 12: Adsorption isotherm for ethane at 318 K predicted with the developed polarizable force field and charges determined via (triangles) DFT calculations, and (diamonds) the QEq method.

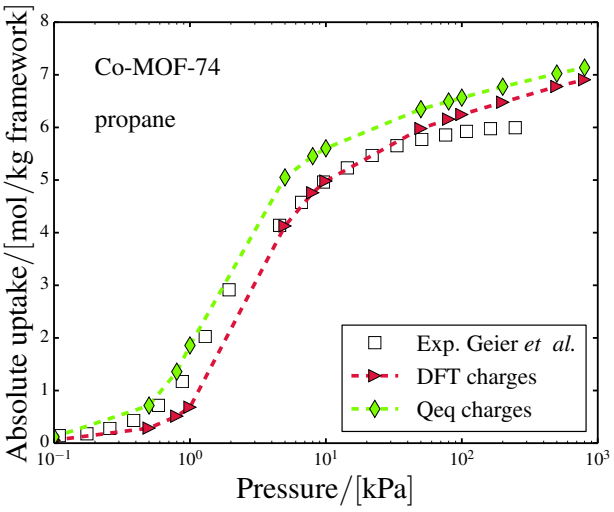

Figure 13: Adsorption isotherm for propane at 318 K predicted with the developed polarizable force field and charges determined via (triangles) DFT calculations, and (diamonds) the QEq method.

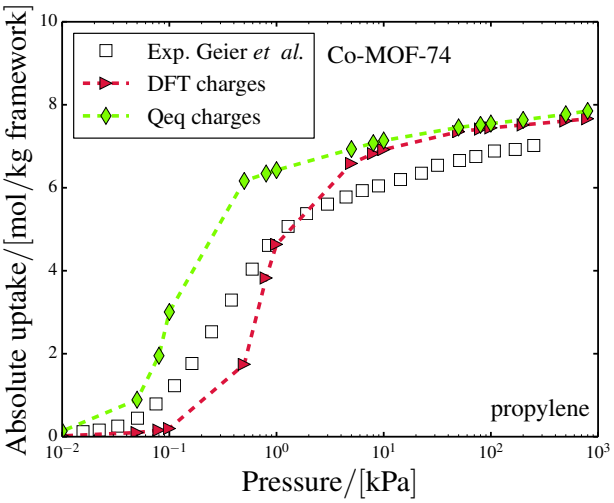

Figure 14: Adsorption isotherm for propylene at 318 K predicted with the developed polarizable force field and charges determined via (triangles) DFT calculations, and (diamonds) the QEq method.

Energy surfaces of Co-MOF-74 for the maximum energy plane in the z-direction

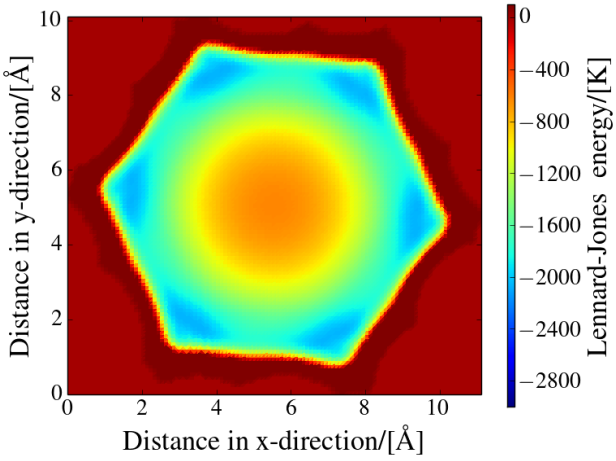

Figure 15: Lennard-Jones energies evaluated on a grid with 0.1 Å spacing on the maximum energy plane in z-direction for ethylene in Co-MOF-74. Grid points for which the total energy (in units of k_B) is larger than 100 K are represented in dark red.

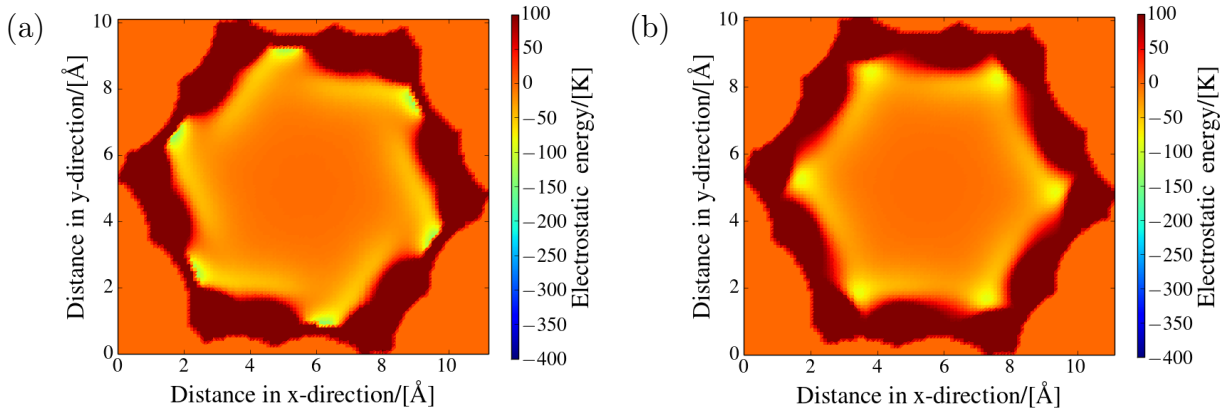

Figure 16: Comparison between the electrostatic energies for ethylene in Co-MOF-74 on a grid with (a) DFT charges and (b) charges calculated with the QEq method for the plane of maximum energy. Grid points for which the total energy (in units of k_B) is larger than 100 K are represented in dark red.

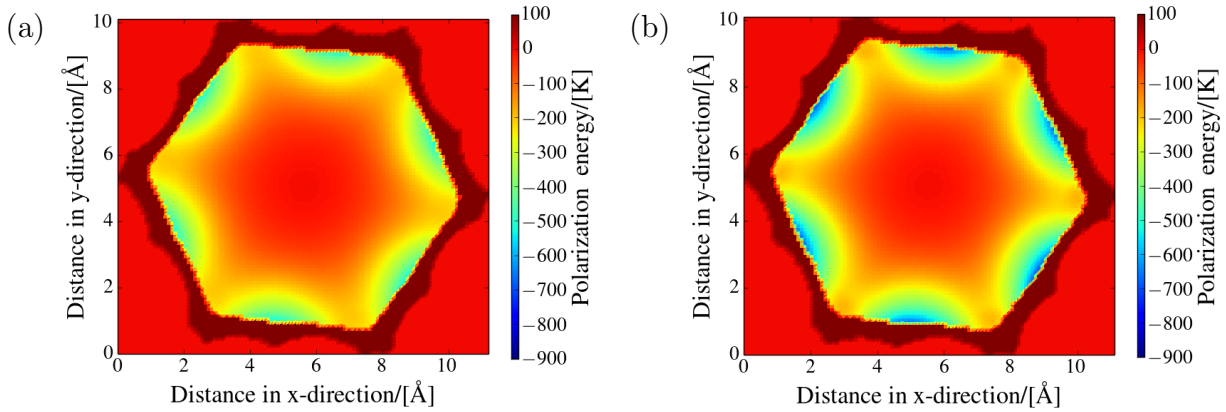

Figure 17: Comparison between the polarization energies for ethylene in Co-MOF-74 on a grid with (a) DFT charges and (b) charges calculated with the QEq method for the plane of maximum energy. Grid points for which the total energy (in units of k_B) is larger than 100 K are represented in dark red.

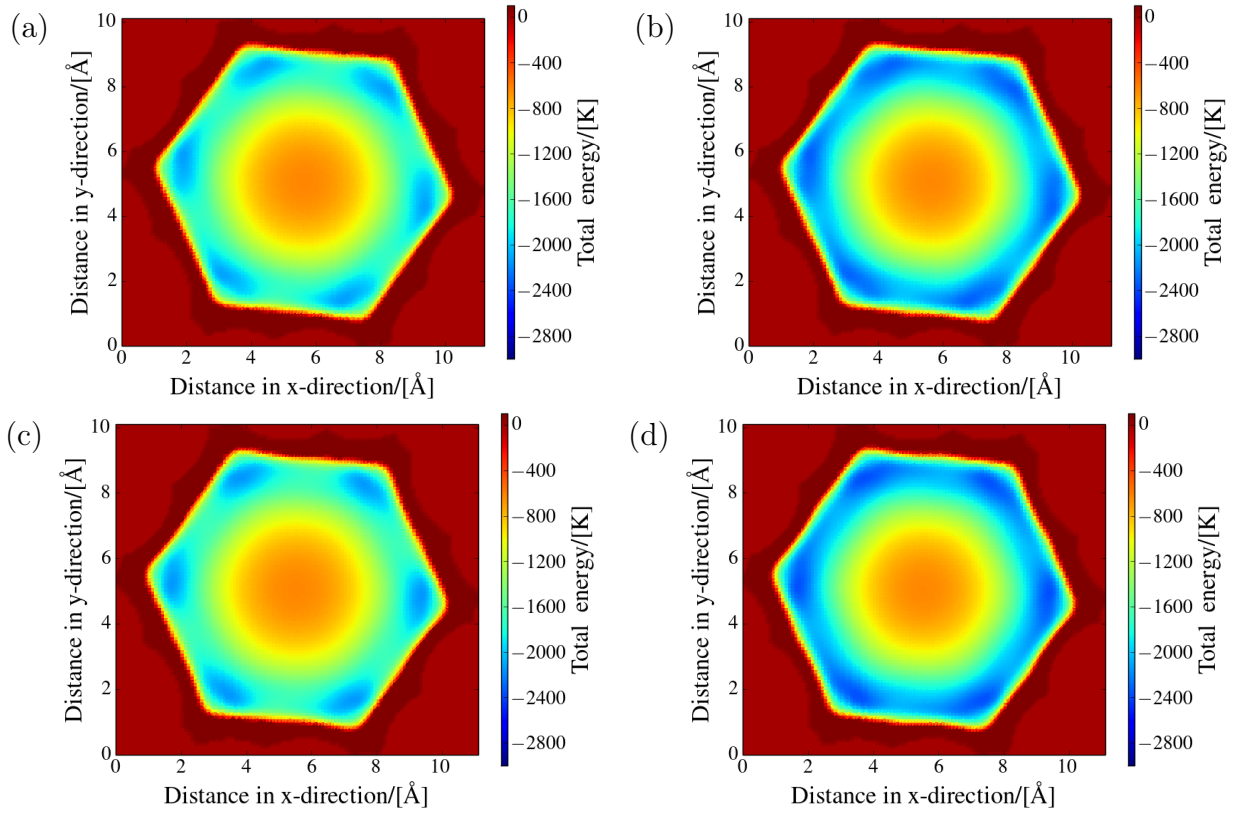

Figure 18: Comparison between the total energies for ethylene in Co-MOF-74 on a grid (left) without and (right) with explicit consideration of polarization energy. Energies calculated with (a) and (b) DFT charges and (c) and (d) charges calculated with the QEq method for the plane of maximum energy. Grid points for which the total energy (in units of k_B) is larger than 100 K are represented in dark red.

References

(1) B. Liu, B. Smit, F. Rey, S. Valencia and S. Calero, *J. Phys. Chem. C* **2008**, *112*, 2492–2498.

(2) L.-C. Lin, K. Lee, L. Gagliardi, J. B. Neaton and B. Smit, *J. Chem. Theory Comput.*, 2014, **10**, 1477–1488.

(3) K. Lee, J. D. Howe, L.-C. Lin, B. Smit and J. B. Neaton, *Chem. Mater.*, 2015, **27**, 668–678.

(4) R. Mercado, B. Vlaisavljevich, L.-C. Lin, K. Lee, Y. Lee, J. A. Mason, D. J. Xiao, M. I. Gonzalez, M. T. Kapelewski, J. B. Neaton and B. Smit, *J. Phys. Chem. C*, 2016, **120**, 12590–12604.

(5) J. M. Stout and C. E. Dykstra, *J. Am. Chem. Soc.*, 1995, **117**, 5127–5132.

(6) C. D. Wick, M. G. Martin and J. I. Siepmann, *J. Phys. Chem. B*, 2000, **104**, 8008–8016.

(7) F. D. Lahoz-Martín, S. Calero, J. J. Gutiérrez-Sevillano and A. Martin-Calvo, *Microporous and Mesoporous Materials*, 2017, **248**, 40–45.

(8) J. J. Gutiérrez-Sevillano, D. Dubbeldam, F. Rey, S. Valencia, M. Palomino, A. Martín-Calvo and S. Calero, *J. Phys. Chem. C*, 2010, **114**, 14907–14914.

(9) S. J. Geier, J. A. Mason, E. D. Bloch, W. L. Queen, M. R. Hudson, C. M. Brown and J. R. Long, *Chem. Sci.*, 2013, **4**, 2054–2061.

(10) A. K. Rappe and W. A. Goddard, *J. Phys. Chem.* **1991**, *95*, 3358–3363.

(11) E. Haldoupis, S. Nair and D. S. Sholl, *J. Am. Chem. Soc.*, 2012, **134**, 4313–4323.